JPET Fast Forward. Published on May 18, 2010 as DOI: 10.1124/jpet.110.167692

Mammalian Target of Rapamycin Pathway Promotes Tumor-Induced Angiogenesis in Adenoid Cystic Carcinoma: Its Suppression by Isoliquiritigenin through Dual Activation of c-Jun NH_2-Terminal Kinase and Inhibition of Extracellular Signal-Regulated Kinase

Zhi-Jun Sun[1], Gang Chen[1], Wei Zhang, Xiang Hu, Cong-Fa Huang, Yu-Fan Wang, Jun Jia, and Yi-Fang Zhao

The State Key Laboratory Breeding Base of Basic Science of Stomatology & Key Laboratory of Oral Biomedicine Ministry of Education, and Department of Oral and Maxillofacial Surgery, School & Hospital of Stomatology, Wuhan University, Wuhan, China (Z.-J.S., G.C., W.Z., X.H., C.-F.H., Y.-F.W., J.J. Y.-F.Z.)

JPET Fast Forward. Published on May 18, 2010 as DOI: 10.1124/jpet.110.167692
This article has not been copyedited and formatted. The final version may differ from this version.

Running Title: Isoliquiritigenin Targets mTOR in Adenoid Cystic Carcinoma

Address correspondence to: Yi-Fang Zhao, Department of Oral and Maxillofacial Surgery, School and Hospital of Stomatology, Wuhan University, Wuhan 430079, China.

Phone: 86-27-87686158; Fax: 86-27-87873260; E-mail: yifang@whuss.com;

Number of text Page: 40

Number of tables: 1

Number of figures: 7

Number of references: 40

Number of words in the Abstract: 250

Number of words in the Introduction: 489

Number of words in the Discussion: 1492

ABBREVIATIONS: ISL, isoliquiritigenin; ACC, adenoid cystic carcinoma; mTOR, mammalian target of rapamycin; MAPK, mitogen-activated protein kinase; JNK, c-Jun NH_2-terminal kinase; ERK, extracellular signal-regulated kinase; NF-κB, nuclear factor-κB; IKK, IκBα kinase; GSK, glycogen synthetase kinase; VEGF, vascular endothelial growth factor; b-FGF, basic fibroblast growth factor; G-CSF, granulocyte colony stimulating factor; PDGF, platelet-derived growth factor; MVD, microvessel density; CM, conditioned medium; NSG, normal salivary gland; PBS, phosphate-buffered saline; TSC, tuberous sclerosis complex; GAP, GTPase-activating protein; CAM, chick chorioallantoic membrane; ANOVA, one-way analysis of variance.

Section Recommendation:

Cellular and Molecular

JPET Fast Forward. Published on May 18, 2010 as DOI: 10.1124/jpet.110.167692
This article has not been copyedited and formatted. The final version may differ from this version.

ABSTRACT

Tumor-induced angiogenesis is essential for invasive growth and hematogenous metastasis of adenoid cystic carcinoma (ACC), a highly aggressive neoplasm mostly occurring in salivary glands. Previous studies have indicated that strategies directed against angiogenesis will help develop new therapeutics for ACC. The Chinese folk medicine licorice has been used for years as a natural remedy for angiogenesis-related diseases. Here we examined the effects of isoliquiritigenin (ISL), a flavonoid isolated from licorice, on the growth and viability of ACC cells, and observed a concentration-dependent (0-20 μM) inhibition of cell growth without cell death at 24 h. In a further mimic co-culture study, ISL effectively suppressed the ability of ACC cells to induce *in vitro* proliferation, migration and tube formation of human endothelial hybridoma (EAhy926) cells as well as *ex vivo* and *in vivo* angiogenesis, whereas it exerted no effect on EAhy926 cells when added directly or in the presence of vascular endothelial growth factor (VEGF). The data also showed that the specific suppression of tumor-angiogenesis by ISL was due to down-regulation of mTOR pathway-dependent VEGF production by ACC cells, correlating with concurrent activation of c-Jun NH_2-terminal kinase (JNK) and inhibition of extracellular signal-regulated kinase (ERK). Most Importantly, ISL also significantly decreased the microvessel density (MVD) within xenograft tumors, associating with the reduction of VEGF production and suppression of mTOR pathway co-regulated by JNK and ERK, as revealed by immunohistochemical studies and clustering analysis. Collectively, our results highlight that ISL is a novel inhibitor of tumor-angiogenesis that possesses great therapeutic potential for ACC.

Introduction

Adenoid cystic carcinoma (ACC) is a glandular epithelial malignancy, which frequently arises in secretary glands especially the major and minor salivary glands. This neoplasm often presents a prolonged clinical course, and is characterized by its infiltrative nature, high incidence of distant metastasis as well as poor long-term survival rate (Spiro, 1997). Nevertheless, up to now, there is no effective strategy existing for the treatment against ACC. Currently, curative surgery followed by postoperative radiotherapy and/or chemotherapy is the preferred therapeutics for ACC. However, it has been demonstrated ineffective for locally recurrent and distantly metastatic ACC. Thus, novel therapeutic approaches to control the development and metastasis of ACC are urgently needed.

Angiogenesis, the formation of new blood vessels from the endothelium of the existing vasculature, has been widely accepted to play a critical role in tumor progression and metastasis (Folkman, 1990; Hanahan and Folkman, 1996). Avascular tumors can rarely grow beyond 2 to 3 mm in diameter because of the diffusion limit for oxygen and nutrients (Dhanabal et al., 2005). However, once tumors become capable of angiogenesis, they can grow rapidly and metastasize (Lin et al., 2007). Thus, anti-angiogenic therapy has regarded as one of the most promising approaches to control tumor growth, invasiveness, as well as metastasis (De Smet et al., 2006). However, to our best knowledge, the significance of anti-angiogenic strategies in therapeutics against ACC, a highly aggressive tumor with exuberant angiogenesis (Zhang et al., 2005; Zhang and Peng, 2009), has not been explored and clarified.

Based on the above concerning, we expected that identification and preclinical/clinical development of novel agents that are nontoxic but can specifically suppress tumor-induced angiogenesis might be a rational approach to develop effective therapies against ACC. Of note, epidemiological studies have indicated that dietary uptake of flavonoids, a large group of polyphenolic compounds present in most fruits, vegetables, and beverages, is associated with a low risk of cancer (Chang et al., 2008). Isoliquiritigenin (ISL), 2', 4', 4'-three hydroxy chalcone (Fig. 1), is one such naturally occurring flavonoid which has shown to be nontoxic to humans but have various biological properties, such as anti-inflammation, antioxidant, anti-platelet aggregation, as well as vasorelaxant and estrogenic effects (Chen et al., 2009). In addition, ISL has also been demonstrated to possess significant anti-tumor activities including proliferation-inhibition and /or apoptosis-induction (Jung et al., 2006), as well as metastasis-prevention (Yamazaki et al., 2002). However, there is no study focusing on the pharmacological activity of ISL in tumor-induced angiogenesis, a frequently mentioned anti-tumor target for some other flavonoids. Meanwhile, it is also worthwhile to mention that the Chinese folk medicine licorice, from which ISL is derived, has been used for years as a natural remedy for angiogenesis-related diseases. Therefore, in the present study, we explored the effects of ISL on ACC-induced angiogenesis, attempting to address whether the anti-tumor activities of ISL is due, at least in part, to its suppression of tumor-induced angiogenesis and more importantly to develop novel therapeutics against ACC.

Methods

Materials. Unless otherwise noted, all chemicals and reagents including ISL were purchased from Sigma-Aldrich (St. Louis, MO). Recombinant human VEGF ($VEGF_{165}$) was from R&D Systems (Minneapolis, MN). Primary antibodies for phospho-Akt (Ser473), Akt, phospho-mTOR (Ser2448), mTOR, phospho-ERK1/2 (Thr202/Tyr204), ERK1/2, phospho-p38 MAPK (Thr180/Tyr182), p38 MAPK, Phospho-JNK1/2 (Thr183/Tyr185), JNK1/2, phospho-S6 (Ser235/236), S6, phospho-TSC2 (Thr1462) were purchased from Cell Signaling Technology (Danvers, MA). Primary antibodies against β-actin, mouse CD31, as well as human CD34, NF-κB p65 and VEGF were purchased from Santa Cruz (Santa Cruz, CA).

Patients and immunohistochemistry. Fifty pathologically confirmed human ACC specimens, with corresponding 6 pericancerous normal salivary gland (NSG) tissues were collected at Hospital of Stomatology, Wuhan University, P.R.China. All specimens were fixed in 4% buffered paraformaldehyde and embedded in paraffin. The procedures were performed in accordance to the guidelines of the National Institutes of Health guidelines regarding the use of human tissues. The study was approved from the review board of the Ethics Committee of Hospital of Stomatology, Wuhan University. The immunohistochemical analyses were performed according to our previous procedures (Sun et al., 2010). Paraffin embedded specimens were serially cut into 4-μm sections, deparafinized, and antigen retrieved by microwave. After that, the sections were washed with phosphate-buffered saline (PBS) and incubated within 3% hydrogen peroxide and 10% goat or rabbit serum for 15 min, followed by an overnight incubation, either with p-TSC2 (1:200), p-mTOR (1:200), p-S6 (1:200), VEGF

(1:100), and CD34 (1:200) antibody. The antibody binding was detected by horseradish peroxidase-conjugated secondary antibody using diaminobenzidine substrate kit (Dako, Carpinteria, CA) according to the manufacturer's protocol. While the negative control slides were obtained by using PBS buffer instead of the primary antibody. Positive controls were oral squamous cell carcinoma slides known to have positive staining for p-mTOR, p-S6, VEGF, and CD34. For each section, at least five fields with typical pathological changes were randomly selected and counted at a magnification of 400 with light microscope (Leica, Wetzlar) by two independent observers (Z.J. Sun and G. Chen) blindly. For p-TSC2, p-mTOR, p-S6 and VEGF, the staining scores were evaluated as the summation of staining intensity (0, no staining; 1, mild staining; 2, moderate staining; and 3, intense staining) and the percentage of positive cells (0, <10%; 1, 10%-25%; 2, 25%-50%; 3, 50-75%; and 4, 75-100% of stained cells) (Zhang et al., 2005). For MVD, the results were calculated according to a modified method based on the technique described by Weidner et al. (Weidner et al., 1991).

Double-labeling immunofluorescence histochemistry. Double-labeling immunofluorescence histochemistry was performed on formalin-fixed, paraffin-embedded 5-μm sections. Briefly, the tissue sections were dewaxed in xylene, hydrated through graded alcohols and distilled water, and washed thoroughly with PBS. Antigen retrieval was done using 10 mM citrate buffer (pH 6.0) in a microwave oven for 20 min. The sections were allowed to cool down and rinsed twice with PBS, and then incubated in 3% hydrogen peroxide in PBS for 30 min, followed by another incubation in 10% nonimmune donkey serum (Sigma) for 1 h at room temperature. After that, excess solution was discarded and the sections incubated with

p-S6 (1:100) and VEGF (1:50) antibodies together overnight at 4 °C. After washing with PBS, the sections were sequentially incubated with FITC-conjugated donkey anti-rabbit antibody and TRITC-conjugated donkey anti-mouse antibody (Jackson Immunoresearch Labs, West Grove, PA; 1:200), respectively, for 1 h. Nuclei were counterstained with DAPI, followed by observation under a fluorescence microscope (Leica).

Cell culture and conditional medium collection. The high (ACC-M) and low (ACC-2) metastasis cell lines of human ACC (Guan et al., 1997) and human endothelial hybridoma cell line EAhy926 were obtained from the China Center for Type Culture Collection, and were maintained in DMEM containing 10% FBS, 100 U/mL penicillin, and 100 μg/mL streptomycin. The cells were incubated in a humidified atmosphere of 95% air and 5% CO_2 at 37 °C.

The collection of ACC conditional medium (CM) was performed as previous described (Ali et al., 2007) with minor modification. Briefly, when ACC cells were grown to 70% confluence after overnight incubation, they were starved in serum-deprived DMEM medium for 12 h to obtain cell synchronization (Zhang and Peng, 2009). Then the serum-deprived medium was discarded, and the cells were exposed to indicated concentrations of ISL in fresh DMEM medium containing 10% FBS for 24 h. After that the cells were washed thoroughly with PBS and further incubated in serum-deprived DMEM for another 24 h, and then the cleared supernatants were collected as the CM and stored at -80 °C.

Cell growth analysis and cell viability measurement. The growth curves of ACC cells were measured by Cell Titer-Glo (CTG; Promega, Madison, WI) luminescent assay. In brief, both

ACC-2 and ACC-M cells (5000 cells/well) were seeded in a 96-well microplate (Corning, Acton, MA) in a final volume of 100 µl. After overnight incubation, indicated concentrations of ISL in fresh DMEM medium containing 10% FBS were added and incubated for 24, 48, or 72 h. After completion of the treatment, 100 µl of CTG solution was added to each well and incubated for 20 minutes at room temperature in dark. Lysate (50 µl) was transferred to a 96-well white plate (Greiner Bio-One, Frickenhausen), and then the luminescence was measured. Percent cell growth was calculated by considering 100% growth at the time of ISL addition.

In the cell viability assays, ACC or EAhy926 cells (3×10^5) was seeded in 6 cm dishes. Experimental conditions were the same as mentioned in the CTG assay, and the cell viability was measured using the Vi-cell cell viability analyzer (Beckman coulter, Fullerton). The relative cell viability was represented as a percentage of the control group.

Wound healing assay. EAhy926 cells were seeded in 6-well culture plates (Corning) and allowed to 90% confluence, followed by the addition of CM. The center of the cell monolayers were scraped with a sterile micropipette tip to create a gap of constant width. After 12 h, the cells migrated in the gap were counted after fixed and observed under a phase microscope.

Boyden chamber migration assay. The migration of endothelium cells was also measured Transwell Boyden chamber (Corning) containing a 6.5 mm diameter polycarbonate filter (pore size of 8 µm). Starved EAhy926 cells (2×10^4 cells/well) were seeded on the upper wells in 100 µl of serum-deprived medium, whereas CM was applied to the lower wells as chemoattractant. After incubation for 12 h at 37 °C, the cells in the upper surface of the membrane were

JPET Fast Forward. Published on May 18, 2010 as DOI: 10.1124/jpet.110.167692
This article has not been copyedited and formatted. The final version may differ from this version.

carefully removed with a cotton swab, and migrated cells were fixed with methanol, stained with crystal violet, and then photographed and counted.

Capillary-like tube formation assay. Capillary-like tube formation assay was also performed to examine the effect of ISL on ACC-induced angiogenesis *in vitro.* EAhy926 cells (2×10^5 cell/dish) in CM were seeded into 6 cm culture dishes coated with Matrigel (BD Biosciences, Bedford, MA) and incubated for 24 h at 37 °C. After that the cells were fixed and stained with Acridine Orange. The formation of capillary-like structure was captured, and the tubes were scanned and quantitated using Image-Pro Plus (Media Cybernetics, Bethesda, MD).

Rat Aortic Ring Assay. The thoracic aortas were harvested from Sprague Dawley rats (6 weeks of age) and placed in the 48-well plates coated with 120 μl of Matrigel (BD Biosciences) and sealed in place with an overlay of 50 μl of Matrigel. Conditioned medium treated with or without ISL was added to the wells in a final volume of 200 μl. As controls, medium alone was assayed. On days 6, the microvessel outgrowth was photographed under a phase microscope. The assay was scored from 0 (least positive) to 5 (most positive) in a double-blinded manner.

Chicken chorioallantoic membrane assay. A modified chick chorioallantoic membrane (CAM) assay was carried out as previously described (Kim et al., 2002). Briefly, the sterile filter paper discs (8 mm) containing 20 μl CM with or without ISL treatment were placed on the CAM of a 9-day-old embryo. After 72 h incubation, the area around the discs was photographed with a stereo microscope, and the number of newly formed vessels was counted by two observers

JPET Fast Forward. Published on May 18, 2010 as DOI: 10.1124/jpet.110.167692
This article has not been copyedited and formatted. The final version may differ from this version.

in a double-blind manner. Each assay takes 8-10 eggs.

Matrigel Plug Assay. *In Vivo* Matrigel plug assay was performed as described previously (Passaniti, 1992). Briefly, 0.6 mL Matrigel containing 0.2 mL CM was injected subcutaneously into nude mice. After 7 days, the skin of the mouse was pulled back to expose the Matrigel plug completely. The plugs were photographed and then hemoglobin was measured using the Drabkin reagent kit 525 (Sigma) for the quantification of blood vessel formation.

Semi-quantitative reverse transcription-PCR. To evaluate the mRNA expression of growth factors in ACC cells after ISL treatment, semi-quantitative reverse transcription (RT)-PCR was performed. Briefly, ACC-M cells were exposed to indicated concentrations of ISL in DMEM medium containing 10% FBS for 24 h, and then total RNA from the cells was isolated with TRIZOL Reagent (Invitrogen). Aliquots (1 μg) of RNA were reverse transcribed to cDNA (20 μL) with Oligo dT and AMV reverse transcriptase (Takara, Japan). One-fifth of the cDNA was used as a template for PCR using a PE9700 RT-PCR system (Applied Biosystems). The primer sequences for PCR were designed as follows: VEGF: 5'-TCATCTCTCCTATGTGCTGGC-3' and 5'-ATGAACTTTCTGCTCTCTGG-3'; basic fibroblast growth factor (b-FGF): 5'-GTGTGTGCTAACCGTTACCT-3' and 5'-GCTCTTAGCAGACATTGGAAG-3'; granulocyte colony stimulating factor (G-CSF): 5'-AGACAGGGAAGAGCAGAACGG-3' and 5'-GCCAGAGTGAGGGGTGCAA-3'; platelet-derived growth factor (PDGF): 5'-CCCCTGCCCATTCGGAGGAAGAG-3' and 5'-TTGGCCACCTTGACGCTGCGGTG-3'; GAPDH (control): 5'-AACGGATTTGGTCGTATTGGG-3' and

5'-CAGGGGTGCTAAGCAGTTGG-3'. The PCR products were electrophoresed in 2% agarose gel and visualized with ethidium bromide. The intensity of each band was analyzed densitometrically using Gene Tools software (Syngene, Cambridge, UK).

ELISA assays for secretion of growth factors. ACC-M cells were starved in serum-deprived DMEM medium for 12 h to obtain cell synchronization. Then the serum-deprived medium was discarded, and the cells were exposed to indicated concentrations of ISL in fresh DMEM medium containing 10% FBS for 24 h. After that the cells were washed thoroughly with PBS and further incubated in serum-deprived DMEM medium for another 24 h to allow angiogenic factor production. Subsequently, the culture medium was collected and used to determine the secretion of VEGF, bFGF, G-CSF, and PDGF using commercially available kits (R&D Systems) according to the manufacturers' recommendations.

Western blot analysis. ACC-M cells were treated with indicated concentrations of ISL in DMEM medium containing 10% FBS for 24 h. Then the cells were lysed and the total protein was separated using a 10% sodium dodecylsulfate-polyacrylamide gel electrophoresis (SDS-PAGE) and transferred on polyvinylidene fluoride membranes (Millipore, Billerica, MA). The immunoblots were cultured overnight at 4 °C with the corresponding primary antibodies in blocking solution, followed by incubation with horseradish peroxidase-conjugated secondary antibody (Pierce, Rockford, IL) respectively. Then blots were developed by a Super Enhanced chemiluminescence detection kit (Applygen Technologies Inc., Beijing). β-actin was detected on the same membrane and used as a loading control.

JPET Fast Forward. Published on May 18, 2010 as DOI: 10.1124/jpet.110.167692
This article has not been copyedited and formatted. The final version may differ from this version.

Nude Mice Xenografts. Female BALB/c nude mice (18-20 g; 6-8 weeks of age) were purchased from the Experimental Animal Center of Wuhan University in pressurized ventilated cage according to institutional regulations. All studies were approved and overseen by Local Institutional Animal Care and Use Committee. ACC-M cells (2×10^6 in 0.2 mL medium) were collected from subconfluent cultures and inoculated s.c. into the flank of the mice. After 7 days, tumor-bearing mice were randomly divided into three groups, which were respectively given with corn oil (Control, 100 μL, p.o., daily; n=8), low dose of ISL (0.5 g/kg, p.o., daily; n=8) or high dose of ISL (1 g/kg, p.o., daily; n=8) for 30 consecutive days. Tumor growth was determined by measuring the size of the tumors daily for 30 days. Tumor volumes were calculated according to the formula ($width^2 \times length$) / 2. The mice were euthanatized at Day 30, and the tumors were captured, photographed, and then embedded in paraffin for MVD detection and immunohistochemical analysis.

Microvessel density in xenograft tumor samples. To quantify angiogenesis in xenograft tumor samples, microvessels were identified by CD31 immunofluorescence staining. The CD31 stained section were observed under a Leica fluorescence microscope, and images were captured from different areas in each section. Then the images were processed using Image-Pro Plus, and the vessel density was estimated by measuring the pixel intensity in each field of view. The vessel density of each group was represented as intensity per pixel. A total of 20 high power fields were examined from three tumors of each of the treatment groups.

Hierarchical clustering, data visualization, and statistical analysis. The staining scores that resulted from immunohistochemical analyses of xenografts tumor samples were converted into scaled values centered on zero in Microsoft excel. The hierarchical analysis was done using Cluster 3.0 (http://bonsai.ims.u-tokyo.ac.jp/~mdehoon/software/cluster/) with average linkage based on Pearson's correlation coefficient as the selection variable on the unsupervised approach (Eisen et al., 1998). The results were visualized using the Java TreeView 1.0.5 (http://jtreeview.sourceforge.net/) as previously described (Saldanha, 2004). The clustered data were arranged with markers on the horizontal axis and tissue samples on the vertical axis. Two biomarkers with a close relationship are located next to each other.

All data were expressed as mean ± SEM of three independent experiments. One-way analysis of variance (ANOVA), Student-Newman-Keuls, and Spearman rank correlation test were used for statistical analysis. $P < 0.05$ was considered significantly different.

Results

ISL inhibits the growth of ACC cells and prevents ACC-induced proliferation of EAhy926 cells. In this study, we initially determined the growth characteristics of both ACC-M and ACC-2 cells in response to ISL treatment using the CTG assay. As shown in Fig. 2A and 2B, ISL (0-20 μM) concentration- and time-dependently decreased the growth activity of both ACC-M and ACC-2 cells, but more prominent in ACC-M cell line. Moreover, results from the cell viability assays (Fig. 2C and 2D) revealed that treatment with increased concentrations of ISL (5, 10 and 20 μM) at 24 h did not affect the viability of both ACC-M and ACC-2 cells, indicating that the growth inhibitory effect of ISL at 24 h was not associated with the cytotoxicity. In contrast, significant decrease of ACC cell viability was noticed after treatment with higher concentrations of ISL (10 and 20 μM) for 48 h and 72 h. Thus, the 24 h treatment period of ISL (0, 5, 10 and 20 μM) was selected as the nontoxic treatment condition used in the CM collection and following studies.

Angiogenesis is a complex biological process that requires the precise coordination of multiple and various steps, including endothelial cell proliferation, migration, and tube formation (Folkman, 1995; Bussolino et al., 1997). To ascertain the inhibitory effect of ISL on tumor-induced angiogenic features of endothelium cells, a set of angiogenesis assays *in vitro* was performed. Firstly, we explored the effect of ISL on ACC-induced EAhy926 cell proliferation. The number of EAhy926 cells was measured in absence or presence of CM with or without indicated concentrations of ISL. As shown in Fig. 2E and 2F, CM without ISL treatment significantly increased viable EAhy926 cell number. However, pretreatment with ISL effectively blocked CM-induced proliferation of EAhy926 cells in a concentration-dependent

manner. Meanwhile, we also found that this preventive effect of ISL is more prominent in ACC-M cell line, consistence with the results from cell growth analyses. We next tried to explore the anti-proliferation effect of ISL on untreated and VEGF-treated EAhy926 cells. But as the results shown, treatment with ISL showed no influence on the proliferation of untreated or VEGF-treated EAhy926 cells. These findings initially indicated that ISL may only selectively targets tumor-induced angiogenic process.

ISL inhibits ACC-induced endothelial cell migration and tube formation. Since cell migration is necessary for the angiogenic process of endothelial cells, we then investigated the effect of ISL on ACC-induced EAhy926 cell migration. Results from the wound healing assays revealed that ISL concentration-dependently prevented CM-induced mobility of EAhy926 cells (Fig. 3A). Additionally, the Boyden Chamber assay also confirmed the preventive effects on ACC CM-induced EAhy926 cell migration (Fig. 3A).

It is also well known that endothelial cells can form capillary-like structures spontaneously on Matrigel, which is crucial in vasculogenesis. Therefore, we further detected the effect of ISL on ACC-induced tube formation of EAhy926 cells. CM pretreated with or without indicated concentrations of ISL was added the Matrigel-coated dishes seeded with EAhy926 cells. The total number of branched tubes per field was counted after 24 h incubation. As the results (Fig. 3A), CM without ISL treatment significantly promoted the capillary structure formation of EAhy926 cells when compared with the negative controls. However, the induced tube formation was effectively prevented by pretreatment with ISL in a concentration-dependent manner.

JPET Fast Forward. Published on May 18, 2010 as DOI: 10.1124/jpet.110.167692
This article has not been copyedited and formatted. The final version may differ from this version.

In addition, our results also revealed that ISL failed to affect the migration and tube formation of untreated or VEGF-treated EAhy926 cells, repeatedly demonstrating that ISL only selectively suppressed tumor-induced angiogenic process, but showed no influence on pre-existing normal angiogenesis (Fig. 3B). Also all the above results revealed that the tumor-angiogenesis prevention activity exerted by ISL *in vitro* is more prominent in the high metastasis cell line ACC-M when compared with that in the low metastasis cell line ACC-2, suggesting high specificity. Thus, the ACC-M cell line was chosen for the subsequent studies.

ISL prevents ACC-induced angiogenesis *ex vivo* and *in vivo*. To verify the preventive effect of ISL on ACC-induced angiogenesis *in vitro*, a series of *ex vivo and in vivo* assays were further carried out. Firstly, we performed the *ex vivo* aortic ring assays using isolated aortas from mice. The 1-mm-long to 1.5-mm-long aortic rings were put on Matrigel and covered by another Matrigel layer, followed by addition of ACC-M CM with or without ISL pretreatment. After incubation for 6 days, the microvessel outgrowth from the aortic rings was analyzed. As shown in Fig. 3C, the results demonstrated that ISL at 20 μM nearly blocked all the new microvessel outgrowth induced by CM from ACC-M cells.

The ability of ISL to prevent *in vivo* ACC-induced angiogenesis was next examined using the CAM assay and Matrigel plug assay. In the CAM assays, paper discs were prepared and swamped into ACC-M CM treated with or without ISL, and then placed on the surface of CAM. At the end of treatment, the newly formed microvessels around the loaded disk were counted and analyzed. As shown in Fig. 3D, the results revealed that treatment with 20 μM ISL almost revered the stimulated effect of ACC-M CM on new microvessel formation. Furthermore,

JPET Fast Forward. Published on May 18, 2010 as DOI: 10.1124/jpet.110.167692
This article has not been copyedited and formatted. The final version may differ from this version.

results from the Matrigel plug assays (Fig. 3E) also confirmed this conclusion that plugs with ACC CM without ISL treatment appeared dark-red color, however plugs with Matrigel alone or with CM with 20 μM ISL treatment were pretty pale. The hemoglobin content within the Matrigel plugs was measured to quantify the tumor-induced angiogenesis prevention effect of ISL, and the results were shown in Fig. 3E. Taken together, our data for the first time strongly implicated that ISL is a potent and specific inhibitor of tumor-induced angiogenesis in ACC.

ISL down-regulates VEGF production in ACC cells. Angiogenesis is a complex biological process involving a wide variety of regulators. The above results have indicated that ISL possessed high potential to prevent ACC-induced angiogenesis both *in vitro* and *in vivo*. In order to further elucidate the mechanisms underlying this preventive effect of ISL, the mRNA expression and protein secretion levels of some key angiogenic factors were tested by the semi-quantitative RT-PCR as well as ELISA assays, respectively. As shown in Fig. 3F and 3G, ISL treatment significantly down-regulated VEGF production in both mRNA expression and protein secretion levels. However, the production of bFGF, G-CSF, or PDGF was not altered (data not shown). Indeed, VEGF is generally considered to be the most potent and specific angiogenic factor that closely associated with the angiogenic process in ACC. Thus, it is rational that ISL down-regulated the VEGF production by ACC cells and led to the prevention of angiogenesis-induction.

ISL inactivates the mTOR signaling pathway co-regulated by JNK and ERK. To unmask the precise molecular mechanisms underlying the above demonstrated inhibitory activities of

JPET Fast Forward. Published on May 18, 2010 as DOI: 10.1124/jpet.110.167692
This article has not been copyedited and formatted. The final version may differ from this version.

ISL, a set of western blot analyses was performed. The data revealed that ISL significantly suppressed the phosphorylation of mTOR, S6, and ERK, and meanwhile up-regulated the phosphorylation level of tuberous sclerosis complex (TSC)-2 and JNK (Fig. 4A) in a concentration- and time-dependent manner, but it failed to affect the activation status of PI3K, Akt , p38, as well as nuclear factor-κB (NF-κB) and IκBα kinase (IKK) (data not shown). To further determine the functional significance of mTOR suppression in the inhibitory activities of ISL, the specific inhibitor of mTOR rapamycin was given to ACC-M cells before treatment with ISL. As the results, rapamycin (100 nM) significantly suppressed the activity of mTOR as well its downstream target S6 (Fig. 4B), consistent with the nearly complete blockade of ISL-mediated down-regulation of VEGF production (Fig. 4C) and prevention of ACC-induced tube formation of endothelium cells (Fig. 4D). However, treatment of rapamycin showed no influence on ISL-mediated alteration of TSC, ERK or JNK (Fig. 4B). These results indicated that the mTOR signaling pathway may be a crucial downstream mechanism implicated in the inhibitory activities of ISL in ACC.

To further elucidate the relationship between ISL-induced JNK activation and ERK inactivation, as well as their relevance with the TSC/mTOR/S6 pathway, the specific pharmacological inhibitors of both JNK (SP600125) and ERK (PD98059) were used. As the results shown, pretreatment of SP600125 significantly but partially potentialized the preventive effect of ISL on VEGF production (Fig. 4C) as well as ACC-induced angiogenic process (Fig. 4D). Meanwhile, SP600125 pretreatment also significantly enhanced ISL-mediated TSC2 activation and mTOR/S6 suppression, but not ISL-mediated inhibition of ERK (Fig. 4B). On the other hand, PD98059 partially but significantly abrogated the preventive effect of ISL on VEGF

JPET Fast Forward. Published on May 18, 2010 as DOI: 10.1124/jpet.110.167692
This article has not been copyedited and formatted. The final version may differ from this version.

production as well as ACC-induced tube formation of endothelium cells (Fig. 4C and 4D), and concurrently blocked ISL-mediated TSC2 activation and mTOR/S6 suppression, but not ISL-mediated activation of JNK (Fig. 4B). These data indicated that JNK and ERK might be concurrently but independently involved in ISL-mediated suppression of the TSC2/mTOR/S6 pathway as well as ACC-induced angiogenesis. Nevertheless, the precise mechanisms by which JNK and ERK regulate the TSC2/mTOR/S6 pathway in ACC still need further investigation.

ISL suppresses tumor angiogenesis and prevents tumor growth *in vivo*.

To further authenticate the angiogenesis-prevention and growth-inhibition ability of ISL, ACC-M xenografts in nude mice were established. The results showed that the growth of ACC-M tumors was significantly inhibited by ISL treatment in a dose-dependent manner when compared with the vehicle controls (Fig. 5A and 5B), while no toxicity was observed (Fig. 5C). Correspondingly, down-regulated proliferation activity revealed by positive Ki67 expression, as well as reduced MVD marked as CD31 positive staining were also observed in high dose ISL-treated ACC-M tumors (Fig. 5D). To further correlate these *in vivo* tumor-therapeutic effects of ISL to the mechanisms identified *in vitro*, we then evaluated the activation status of some key signaling pathways in ISL-treated ACC-M tumor tissues by immunohistochemical analyses. As the results shown, a decrease in S6 phosphorylation in ISL-treated tumors clearly contrasted the high activation level of S6 in the control group (Fig. 5D), reflecting the hyperactivity of the mTOR signaling pathway in ACC. Concomitant with the reduction in S6 phosphorylation, we also noted a significant decrease in VEGF production in ISL-treated

tumors (Fig. 5D). Importantly, cluster analysis of the immunohistochemical results indicated the therapeutic significance of ISL treatment. As shown in Fig. 5E, all control samples clustered together. And tissues treated with low dose of ISL (0.5 g/kg) were clustered together and adjacent to the controls. Nearly all samples treated with high dose of ISL (1 g/kg) were closely clustered. From the heat map approach, it was also clear that Ki67, p-mTOR, p-S6 and VEGF clustered together, and p-JNK as well as p-ERK were clustered closely to them, but p-PI3K, p-Akt and p-p38 were distantly clustered. All the above results are consistent with our *in vitro* findings, and repeatedly demonstrated that ISL significantly and specifically suppressed tumor-induced angiogenesis in ACC by inhibiting the mTOR signaling pathway through dual JNK activation and ERK inactivation.

Immunohistochemical analyses of clinical specimens confirmed the high activation status of TSC2/mTOR/S6 pathway as well as its essential role in angiogenesis in ACC. To make our above findings more clinically significant and therapeutically meaningful, we further evaluated the nature activation status of mTOR pathway in ACC, and attempted to explore its relevance with angiogenesis. We initially tested and compared the activation status of mTOR signaling pathway in two ACC cell lines. Of interest, the results revealed that the activation status of mTOR pathway in the high metastasis cell line ACC-M was significantly higher than that in the low metastasis cell line ACC-2 (Fig. 6A), correlating with the relatively higher VEGF-production level (Fig. 6B and 6C) as well as angiogenesis-induction ability (Fig. 6D). Importantly, treatment with rapamycin significantly down-regulated the VEGF production, and obviously prevented the angiogenic process of endothelium cells induced by both ACC-M

and ACC-2 cells, but again more prominent in ACC-M cells (Fig. 6D). The above data indicated that the activation of mTOR pathway in ACC cells might contribute a lot to the angiogenesis-induction potential. To further confirm the above findings in ACC cell cultures, we then assessed the nature activation status of mTOR pathway in ACC tissue specimens and explored its relevance with angiogenesis in the tumors. Representative examples of immunohistochemical results are shown in Fig. 7A. In the selected ACC cases, it was clear that p-S6 was intensely stained in the cytoplasm of most ACC cells accompanied by a strong staining of p-mTOR in the cytoplasm and/or nuclei. In contrast, the staining of p-TSC2 was nearly not detectable. Meanwhile, the positive staining of VEGF was obviously detected in the same area. Additionally, the double-labeling immunofluorescence histochemistry of p-S6 and VEGF further confirmed the concurrence of S6 activation and VEGF production (Fig. 7B) in ACC tissues. Importantly, the Spearman rank test showed significant correlation among the staining level of p-TSC2, p-mTOR, p-S6 and VEGF, as well as MVD (Table 1), strongly implicating that the high activation status of mTOR in ACC might greatly contributed to the exuberant angiogenesis involving the regulation of VEGF production. Collectively, the findings in the ACC cell cultures as well in the ACC tissue specimens were highly consistent, which together revealed that the mTOR signaling pathway is ubiquitously activated and correlated with the exuberant angiogenesis in ACC, and more importantly demonstrated the high therapeutic potential of mTOR inhibition.

Discussion

In the present study, ISL, a flavonoid isolated from licorice, was revealed to be a potent therapeutic agent for ACC. Although this natural flavonoid has been extensively considerate as an anti-neoplastic agent in various human cancers (Hsu et al., 2005; Yoshida et al., 2008; Ye et al., 2009) and shown inhibitory effects on phorbol myristate acetate-induced angiogenic process of endothelial cells (Kang et al., 2010), this is the first study regarding tumor-angiogenesis prevention as an important composition of the anti-tumor mechanisms of ISL. Here we demonstrated for the first time that ISL was a potent inhibitor of tumor-induced angiogenesis in ACC. Initially, by employing the growth analysis and viability measurement, we determined that ISL at the concentrations of 0-20 μM did not induce significant ACC cell death but only effectively decreased the cell growth activity. Further investigation revealed that ISL at these concentrations not only significantly prevented ACC-mediated proliferation, migration, and tube formation of human endothelial hybridoma (EAhy926) cell line *in vitro*, but also suppressed ACC-induced angiogenic process *ex vivo* and *in vivo*. Importantly, ISL obviously decreased the MVD within xenograft tumors, concomitant with the down-regulated proliferative activity of ACC cells. Collectively, the results suggested that ISL possessed great therapeutic potential for ACC due to its function of preventing tumor-induced angiogenesis.

Previous studies have implicated multiple growth factors, such as VEGF, bFGF, G-CSF, and PDGF, in tumor growth, angiogenesis, and metastasis (Slomiany and Rosenzweig, 2006; Passam et al., 2008). Among them, VEGF is generally considered to be the most potent and specific angiogenic factor that closely associated with aggressive human cancer cells, including ACC (Zhang et al., 2005; Zhang and Peng, 2009). The present study revealed that

exposure of ACC cells to ISL resulted in significant down-regulation of VEGF production. In contrast, the production of bFGF, G-CSF, or PDGF was unaffected. Taken together, these results suggested that ISL-mediated suppression of tumor-angiogenesis in ACC is most likely caused by VEGF down-regulation.

Recent research has indicated that NF-κB is tightly involved in the production of VEGF in different cell lines (Josko and Mazurek, 2004; Korkolopoulou et al., 2008; Zhang and Peng, 2009), including ACC cells (Zhang et al., 2005; Zhang and Peng, 2009). Furthermore, several flavonoids including ISL have been reported to inhibit NF-κB activation (Kwon et al., 2007). Thus, it is reasonable to hypothesize that ISL may down-regulate VEGF production and prevent ACC cell-induced angiogenesis through inhibition of NF-κB activation. But unexpectedly, our data showed that ISL failed to inactivate NF-κB as well as its upstream regulator IKK. Thus we turned to explore other possible intracellular signals targeted by ISL, especially those with important role in tumor-angiogenesis. Notably, the TSC/mTOR signaling axis is one such pathway that has been extensively implicated in the angiogenic process during the malignant progression of cancers (Lee et al., 2007). The TSC comprises two subunits, the tumor suppressor genes TSC1 and TSC2. TSC1 stabilizes TSC2 through binding with it, thereby preventing TSC2 from ubiquitination and degradation (Benvenuto et al., 2000). TSC2 acts as a GTPase-activating protein (GAP) to regulate RHEB function through converting RHEB from an active GTP-bound form to an inactive GDP-bound form (Benvenuto et al., 2000). Inactivation of TSC2 represses GAP activity and allows GTP-bound RHEB to accumulate. GTP-bound RHEB is known to activate mTOR, a highly conserved serine/threonine kinase, which in turn phosphorylates and activates S6K, leading to the

activation of downstream mTOR/S6 pathway. Conversely, active TSC2 reduces GTP-bound RHEB accumulation and prevents mTOR and S6 activation. Importantly, activation of the TSC/mTOR signaling pathway has been demonstrated to cause up-regulation of VEGF through increases of both transcription and translation (Klos et al., 2006), leading to promoted angiogenesis, enhanced growth and ultimately to tumorigenesis (Inoki et al., 2005). Indeed, the ubiquitous activation of mTOR pathway, resulting from TSC inactivation, has been revealed to closely associate with the extensive abnormal vasculization in various tumors (Onda et al., 1999; Kwiatkowski et al., 2002; Lee et al., 2007), and strategies specifically against mTOR may mitigate the tumor progression due to the prevention of angiogenesis (Lee et al., 2007). In the present study, we noticed that the activity of mTOR as well as its major downstream target S6 was significantly down-regulated by ISL, and meanwhile the phosphorylation level of TSC2 was obviously up-regulated, demonstrating probably involvement of the TSC2/mTOR/S6 pathway.

To make the above findings more clinically significant and therapeutically meaningful, we explored the nature activation status of mTOR pathway as well as its relevance with angiogenesis in ACC. As the results, immunohistochemical analyses showed that the phosphorylation status of mTOR and S6 are significantly higher in ACC tissues when compared to NSG tissues, correlating with decreased TSC2 activation, up-regulated VEGF production as well as increased MVD. Furthermore, the double-labeling immunofluorescence histochemistry analysis also confirmed the concurrence of S6 activation and VEGF production in ACC tissues. Importantly, the phosphorylation level of TSC2, mTOR and S6 are significantly correlated with each other and also with the VEGF production as well as MVD, as

demonstrated by the Spearman rank test. Of interest, our findings also revealed that the activation status of the TSC/mTOR/S6 signaling pathway in the high metastasis cell line ACC-M was significantly higher than that in the low metastasis cell line ACC-2, correlating with the relatively higher VEGF-production level and angiogenesis-induction ability. Collectively, the data strongly implicated that activation of the mTOR signaling pathway is essential for the angiogenic process during the malignant progression of ACC. To our best knowledge, this is the first time that the mTOR pathway was reported to be ubiquitously activated in ACC, especially revealing its potential role in angiogenesis-promotion. These findings may not only lead to a better understanding of the molecular pathogenesis of ACC, but also provide a basis for a rational approach to develop molecular targeted therapies against this aggressive tumor, just like the ISL treatment reported here. To further validate the above conclusion and meanwhile testify the potential of mTOR inhibition in the anti-angiogenic therapeutics against ACC, we then tested the effect of rapamycin, a specific mTOR inhibitor, on the VEGF production as well as angiogenesis-induction by ACC cells. As expected, rapamycin significantly down-regulated the VEGF production, as well as obviously prevented the angiogenic process of endothelium cells induced by both ACC-M and ACC-2 cells, and again more prominent in ACC-M cells. After taking the above results together, it seems to be a conclusion that ISL-mediated suppression of tumor-angiogenesis in ACC is due, at least in part, to its function of down-regulating the TSC2/mTOR/S6 signaling pathway, which was ubiquitously activated and correlated with the exuberant angiogenesis in ACC.

JPET Fast Forward. Published on May 18, 2010 as DOI: 10.1124/jpet.110.167692
This article has not been copyedited and formatted. The final version may differ from this version.

Serine-threonine kinase Akt (protein kinase B), the direct downstream effector of PI3K, is the most frequently mentioned upstream regulator of the TSC/mTOR signaling pathway. However during the attempt to understand the upstream molecular mechanisms for ISL-induced mTOR inactivation, we unexpectedly found that the activation status of PI3K/Akt pathway was not altered by ISL. Since other upstream signals including IKKβ, glycogen synthetase kinase (GSK), and mitogen-activated protein kinases (MAPKs) could also regulate mTOR activity through Akt-independent pathways (Ma et al., 2005; Lee et al., 2007; Ma et al., 2007; Buller et al., 2008), we examined whether these molecules play roles in ISL-mediated mTOR inhibition. As the results shown, ISL treatment concurrently activated JNK and inactivated ERK in ACC cells, but showed no effect on GSK or p38 MAPK, another subfamily of MAPKs. In an attempt to gain more insights into the underlying mechanisms by employing the specific inhibitors of mTOR (rapamycin), JNK (SP600125), and ERK (PD98059), we unmasked that ISL concurrently but independently activated JNK and inactivated ERK to up-regulate TSC2 activity, respectively, and then resulted in mTOR inhibition in ACC cells. Most importantly, the *in vivo* studies further verified the *in vitro* findings. ISL treatment effectively reduced MVD and prevented the tumor growth of ACC-M cells in nude mouse xenograft model. Meanwhile, immunohistochemical analyses showed that ISL significantly blocked the activation of mTOR pathway and down-regulated the production of VEGF. Furthermore, the cluster analysis revealed that the inactivated mTOR pathway and down-regulated VEGF production closely related to each other, as well as to the JNK activation and ERK inactivation, but showed no correlation with the PI3K/Akt or p38 MAPK signaling pathway. All the above results are consistent with our *in vitro* findings.

JPET Fast Forward. Published on May 18, 2010 as DOI: 10.1124/jpet.110.167692
This article has not been copyedited and formatted. The final version may differ from this version.

In conclusion, the present study demonstrated for the first time that ISL, a natural flavonoid derived from licorice, significantly and specifically suppressed tumor-induced angiogenesis in ACC both *in vitro* and *in vivo*, relating with the inhibition of mTOR signaling pathway through dual JNK activation and ERK inactivation. Most importantly, we revealed, also for the first time, that the mTOR signaling pathway was indeed ubiquitously activated and correlated with the exuberant angiogenesis in ACC. Our findings systematically dissected the effects of ISL on the mTOR signaling pathway in ACC, determined the importance of mTOR inhibition for the anti-angiogenic activity of ISL, and shed new light on the mechanisms of anticancer activities of ISL, as well as implicated its great therapeutic potential for ACC.

References

Ali MA, Choy H, Habib AA and Saha D (2007) SNS-032 prevents tumor cell-induced angiogenesis by inhibiting vascular endothelial growth factor. *Neoplasia* **9**:370-381.

Benvenuto G, Li S, Brown SJ, Braverman R, Vass WC, Cheadle JP, Halley DJ, Sampson JR, Wienecke R and DeClue JE (2000) The tuberous sclerosis-1 (TSC1) gene product hamartin suppresses cell growth and augments the expression of the TSC2 product tuberin by inhibiting its ubiquitination. *Oncogene* **19**:6306-6316.

Buller CL, Loberg RD, Fan MH, Zhu Q, Park JL, Vesely E, Inoki K, Guan KL and Brosius FC, 3rd (2008) A GSK-3/TSC2/mTOR pathway regulates glucose uptake and GLUT1 glucose transporter expression. *Am J Physiol Cell Physiol* **295**:C836-843.

Bussolino F, Mantovani A and Persico G (1997) Molecular mechanisms of blood vessel formation. *Trends Biochem Sci* **22**:251-256.

Chang HL, Wu YC, Su JH, Yeh YT and Yuan SS (2008) Protoapigenone, a novel flavonoid, induces apoptosis in human prostate cancer cells through activation of p38 mitogen-activated protein kinase and c-Jun NH2-terminal kinase 1/2. *J Pharmacol Exp Ther* **325**:841-849.

Chen G, Zhu L, Liu Y, Zhou Q, Chen H and Yang J (2009) Isoliquiritigenin, a flavonoid from licorice, plays a dual role in regulating gastrointestinal motility in vitro and in vivo. *Phytother Res* **23**:498-506.

De Smet F, Carmeliet P and Autiero M (2006) Fishing and frogging for anti-angiogenic drugs. *Nat Chem Biol* **2**:228-229.

Dhanabal M, Jeffers M and Larochelle WJ (2005) Anti-angiogenic therapy as a cancer treatment paradigm. *Curr Med Chem Anticancer Agents* **5**:115-130.

Eisen MB, Spellman PT, Brown PO and Botstein D (1998) Cluster analysis and display of genome-wide expression patterns. *Proc Natl Acad Sci U S A* **95**:14863-14868.

Folkman J (1990) What is the evidence that tumors are angiogenesis dependent? *J Natl Cancer Inst* **82**:4-6.

Folkman J (1995) Angiogenesis in cancer, vascular, rheumatoid and other disease. *Nat Med* **1**:27-31.

Guan XF, Qiu WL, He RG and Zhou XJ (1997) Selection of adenoid cystic carcinoma cell clone highly metastatic to the lung: an experimental study. *Int J Oral Maxillofac Surg* **26**:116-119.

Hanahan D and Folkman J (1996) Patterns and emerging mechanisms of the angiogenic switch during tumorigenesis. *Cell* **86**:353-364.

Hsu YL, Kuo PL, Lin LT and Lin CC (2005) Isoliquiritigenin inhibits cell proliferation and induces apoptosis in human hepatoma cells. *Planta Med* **71**:130-134.

Inoki K, Corradetti MN and Guan KL (2005) Dysregulation of the TSC-mTOR pathway in human disease. *Nature Genetics* **37**:19-24.

Josko J and Mazurek M (2004) Transcription factors having impact on vascular endothelial growth factor (VEGF) gene expression in angiogenesis. *Med Sci Monit* **10**:RA89-98.

Jung JI, Lim SS, Choi HJ, Cho HJ, Shin HK, Kim EJ, Chung WY, Park KK and Park JH (2006) Isoliquiritigenin induces apoptosis by depolarizing mitochondrial membranes in prostate cancer cells. *Journal of Nutritional Biochemistry* **17**:689-696.

Kang SW, Choi JS, Choi YJ, Bae JY, Li J, Kim DS, Kim JL, Shin SY, Lee YJ, Kwun IS and Kang YH (2010) Licorice isoliquiritigenin dampens angiogenic activity via inhibition of MAPK-responsive signaling pathways leading to induction of matrix metalloproteinases. *J Nutr Biochem* **21**:55-65.

Kim YM, Lee YM, Kim HS, Kim JD, Choi Y, Kim KW, Lee SY and Kwon YG (2002) TNF-related activation-induced cytokine (TRANCE) induces angiogenesis through the activation of Src and phospholipase C (PLC) in human endothelial cells. *J Biol Chem* **277**:6799-6805.

Klos KS, Wyszomierski SL, Sun M, Tan M, Zhou X, Li P, Yang W, Yin G, Hittelman WN and Yu D (2006) ErbB2 increases vascular endothelial growth factor protein synthesis via activation of mammalian target of rapamycin/p70S6K leading to increased angiogenesis and spontaneous metastasis of human breast cancer cells. *Cancer Research* **66**:2028-2037.

Korkolopoulou P, Levidou G, Saetta AA, El-Habr E, Eftichiadis C, Demenagas P, Thymara I, Xiromeritis K, Boviatsis E, Thomas-Tsagli E, Panayotidis I and Patsouris E (2008) Expression of nuclear factor-kappaB in human astrocytomas: relation to pI kappa Ba, vascular endothelial growth factor, Cox-2, microvascular characteristics, and survival. *Human Pathology* **39**:1143-1152.

Kwiatkowski DJ, Zhang H, Bandura JL, Heiberger KM, Glogauer M, el-Hashemite N and Onda H (2002) A mouse model of TSC1 reveals sex-dependent lethality from liver hemangiomas, and up-regulation of p70S6 kinase activity in Tsc1 null cells. *Human Molecular Genetics* **11**:525-534.

Kwon HM, Choi YJ, Choi JS, Kang SW, Bae JY, Kang IJ, Jun JG, Lee SS, Lim SS and Kang YH (2007) Blockade of cytokine-induced endothelial cell adhesion molecule expression by licorice isoliquiritigenin through NF-kappaB signal disruption. *Exp Biol Med (Maywood)* **232**:235-245.

Lee DF, Kuo HP, Chen CT, Hsu JM, Chou CK, Wei Y, Sun HL, Li LY, Ping B, Huang WC, He X, Hung JY, Lai CC, Ding Q, Su JL, Yang JY, Sahin AA, Hortobagyi GN, Tsai FJ, Tsai CH and Hung MC (2007) IKK beta suppression of TSC1 links inflammation and tumor angiogenesis via the mTOR pathway. *Cell* **130**:440-455.

Lin HL, Chiou SH, Wu CW, Lin WB, Chen LH, Yang YP, Tsai ML, Uen YH, Liou JP and Chi CW (2007) Combretastatin A4-induced differential cytotoxicity and reduced metastatic ability by inhibition of AKT function in human gastric cancer cells. *J Pharmacol Exp Ther* **323**:365-373.

Ma L, Chen Z, Erdjument-Bromage H, Tempst P and Pandolfi PP (2005) Phosphorylation and functional inactivation of TSC2 by Erk implications for tuberous sclerosis and cancer pathogenesis. *Cell* **121**:179-193.

Ma L, Teruya-Feldstein J, Bonner P, Bernardi R, Franz DN, Witte D, Cordon-Cardo C and Pandolfi PP (2007) Identification of S664 TSC2 phosphorylation as a marker for extracellular signal-regulated kinase-mediated mTOR activation in tuberous sclerosis and human cancer. *Cancer Research* **67**:7106-7112.

Onda H, Lueck A, Marks PW, Warren HB and Kwiatkowski DJ (1999) Tsc2(+/-) mice develop tumors in multiple sites that express gelsolin and are influenced by genetic background. *J Clin Invest* **104**:687-695.

Passam FH, Sfiridaki A, Pappa C, Kyriakou D, Petreli E, Roussou PA and Alexandrakis MG (2008) Angiogenesis-related growth factors and cytokines in the serum of patients with B non-Hodgkin lymphoma; relation to clinical features and response to treatment. *Int J Lab Hematol* **30**:17-25.

Passaniti A (1992) Extracellular matrix-cell interactions: Matrigel and complex cellular pattern formation. *Lab Invest* **67**:804; author reply 804-808.

Saldanha AJ (2004) Java Treeview--extensible visualization of microarray data. *Bioinformatics* **20**:3246-3248.

Slomiany MG and Rosenzweig SA (2006) Hypoxia-inducible factor-1-dependent and -independent regulation of insulin-like growth factor-1-stimulated vascular endothelial growth factor secretion. *J Pharmacol Exp Ther* **318**:666-675.

Spiro RH (1997) Distant metastasis in adenoid cystic carcinoma of salivary origin. *Am J Surg* **174**:495-498.

Sun ZJ, Chen G, Hu X, Zhang W, Liu Y, Zhu LX, Zhou Q and Zhao YF (2010) Activation of PI3K/Akt/IKK-alpha/NF-kappaB signaling pathway is required for the apoptosis-evasion in human salivary adenoid cystic carcinoma: its inhibition by quercetin. *Apoptosis*.

Weidner N, Semple JP, Welch WR and Folkman J (1991) Tumor angiogenesis and metastasis--correlation in invasive breast carcinoma. *N Engl J Med* **324**:1-8.

Yamazaki S, Morita T, Endo H, Hamamoto T, Baba M, Joichi Y, Kaneko S, Okada Y, Okuyama T, Nishino H and Tokue A (2002) Isoliquiritigenin suppresses pulmonary metastasis of mouse renal cell carcinoma. *Cancer Letters* **183**:23-30.

Ye L, Gho WM, Chan FL, Chen S and Leung LK (2009) Dietary administration of the licorice flavonoid isoliquiritigenin deters the growth of MCF-7 cells overexpressing aromatase. *Int J Cancer* **124**:1028-1036.

Yoshida T, Horinaka M, Takara M, Tsuchihashi M, Mukai N, Wakada M and Sakai T (2008) Combination of isoliquiritigenin and tumor necrosis factor-related apoptosis-inducing ligand induces apoptosis in colon cancer HT29 cells. *Environ Health Prev Med* **13**:281-287.

Zhang J and Peng B (2009) NF-kappaB promotes iNOS and VEGF expression in salivary gland adenoid cystic carcinoma cells and enhances endothelial cell motility in vitro. *Cell Prolif* **42**:150-161.

Zhang J, Peng B and Chen X (2005) Expressions of nuclear factor kappaB, inducible nitric oxide synthase, and vascular endothelial growth factor in adenoid cystic carcinoma of salivary glands: correlations with the angiogenesis and clinical outcome. *Clin Cancer Res* **11**:7334-7343.

Footnotes

This study was supported by grants from National Natural Science Foundation of China (30872894 and 30973330) to Prof. Y.F. Zhao and (30801305) to Dr. J. Jia, and the National Undergraduate Innovative Experiment Project (091048654) to Dr. Gang Chen.

[1]Both authors contributed equally to this work.

JPET Fast Forward. Published on May 18, 2010 as DOI: 10.1124/jpet.110.167692
This article has not been copyedited and formatted. The final version may differ from this version.

Legends for Figures

Fig. 1. Molecular structure of ISL. 2', 4', 4'-three hydroxy chalcone.

Fig. 2. Inhibitory effect of ISL on ACC cell growth and viability, as well as ACC-induced proliferation of EAhy926 cells. ACC-M **(A)** and ACC-2 **(B)** cell growth was measured by the CGT assay after treatment with indicated concentrations of ISL in DMEM medium containing 10% FBS for 24, 48, and 72 h. The results were represented as a percentage at the time of ISL addition. ACC-M **(C)** and ACC-2 **(D)** cell viability was measured using the Vi-cell cell viability analyzer after treatment with indicated concentrations of ISL in DMEM medium containing 10% FBS for 24, 48, and 72 h. The results were represented as a percentage of the control group. EAhy926 cell viability after treatment with DMSO (vehicle) alone, ISL alone, VEGF alone, VEGF plus ISL, as well as CM from ACC-M **(E)** or ACC-2 **(F)** cells pretreated with or without ISL was measured using the Vi-cell cell viability analyzer at 24 h. The results were represented as a percentage of the vehicle-treated control group. All data were presented as mean ± SEM from three different experiments with duplicate. *, $P < 0.05$; **, $P < 0.01$ versus the vehicle-treated group; †, $P < 0.05$; ††, $P < 0.01$ versus the CM without ISL treatment group.

Fig. 3. ISL prevents ACC-induced angiogenesis *in vitro*, *ex vivo*, and *in vivo*. **A,** the wound healing assay and Transwell Boyden chamber assay, as well as capillary-like tube formation assay were performed to measure *in vitro* effects of ISL on ACC-induced angiogenic features of EAhy926 cells. The values were represented as a percentage of the vehicle-treated control

group in ACC-2 cell line. **B**, effects of ISL on the angiogenic features of untreated and VEGF-treated EAhy926 cells. **C**, effect of ISL on ACC-induced vessel sprouting in the rat aortic ring assay *ex vivo*. **D**, effect of ISL on ACC-induced angiogenesis in the CAM assay *in vivo*. **E**, effect of ISL on ACC-induced vessel formation in the Matrigel plug assay *in vivo*. The mRNA expression (**F**) and protein secretion (**G**) levels of VEGF were determined by the RT-PCR and ELISA assays, respectively, after incubation with indicated concentrations of ISL for 24 h. All data were presented as mean ± SEM from three different experiments with duplicate. *, $P < 0.05$; **, $P < 0.01$ versus the vehicle-treated group; †, $P < 0.05$; ††, $P < 0.01$ versus the CM without ISL treatment group.

Fig. 4. ISL suppresses the mTOR signaling pathway through dual JNK activation and ERK inactivation. **A**, ACC-M cells were treated with indicated concentrations of ISL in DMEM medium containing 10% FBS for indicated time. The expression levels of p-ERK1/2 (Thr202/Thr204), p-JNK1/2 (Thr183/Thr185), p-TSC2 (Thr1462), p-mTOR (Ser2448) and p-S6 (Ser235/236) as well as their corresponding total protein were determined by Western blot analysis. **B**, ACC-M cells were pretreated with SP600125, PD98059, or rapamycin for 1 h, followed by incubation with ISL for 24 h. The expression levels of p-ERK1/2, p-JNK1/2, p-TSC2 and p-S6 were analyzed by Western blotting. **C** and **D**, ACC-M cells were exposed to SP600125, PD98059, or rapamycin respectively for 1 h, followed by incubation with ISL in DMEM medium containing 10% FBS for 24 h. Then the cells were washed thoroughly with PBS and further incubated in serum-deprived DMEM medium for another 24 h to allow angiogenic factor production. After that the clear supernatant were collected as the CM. The

JPET Fast Forward. Published on May 18, 2010 as DOI: 10.1124/jpet.110.167692
This article has not been copyedited and formatted. The final version may differ from this version.

protein secretion level of VEGF in CM was quantified using the ELISA assay (**C**). Percent VEGF production was calculated by considering 100% production unitedly at the time of ISL addition. When CM was added to EAhy926 cells, the angiogenic activity was measured by the capillary-like tube formation assay (**D**). Percent CM-induced tube formation was calculated by considering 100% formation unitedly at the time of ISL addition. All data were presented as mean ± SEM from three different experiments with duplicate. *, $P < 0.01$ versus the corresponding group without ISL treatment, and † $P < 0.01$ versus the control group with only ISL treatment but without any other pretreatment.

Fig. 5. ISL prevents tumor angiogenesis and growth *in vivo*. **A**, tumor regression observed in ACC xenografts treated with ISL. ACC-M cells were used to establish xenografts in athymic nu/nu mice, and tumor-bearing animals were given with ISL (0.5 or 1 g/kg, p.o., daily; n=8) or corn oil (Vehicle, 100 μL, p.o., daily; n=6) for 30 days. An example of tumor regression in high dose (1 g/kg) ISL-treated animals is depicted. **B**, tumor size from ACC-M xenografts in both ISL- and vehicle-treated groups was assessed daily, as indicated. All values are presented as mean ± SEM (n = 6 or 8). **C**, body weight of mice was measured daily and indicated no side effect of ISL treatment. All values are presented as mean ± SEM (n = 6 or 8). **D**, immunohistochemical analysis of the indicated biomarkers in both control and ISL-treated ACC-M tumor tissues. **E**, hierarchical clustering of immunohistochemical results from the xenograft tumors after treatment with vehicle control (C1-5), low does ISL (ISL-L1-8), and high does ISL (ISL-H1-8). Light yellow, high staining scores; light blue, low staining scores.

Fig. 6. Activation status of the mTOR signaling pathway in both ACC-M and ACC-2 cell lines, as well as its relevance with the angiogenesis-induction ability. **A,** the expression levels of p-TSC2, p-mTOR and p-S6 as well as their corresponding total protein were as well as total protein were determined by Western blot analysis in ACC-M and ACC-2 cell lines, respectively. The mRNA expression (**B**) and protein secretion (**C**) of VEGF in both ACC-M and ACC-2 cell lines, treated with or without rapamycin, were measured by the RT-PCR and ELISA assay, respectively. **D,** the cell migration assay and capillary-like tube formation assay were performed to detect and compare the angiogenesis-induction ability of both ACC-M and ACC-2 cells, as well as their response to rapamycin (Rap) treatment. The results were represented as a percentage of the control group. All data are presented as mean ± SEM from three different experiments with duplicate. Values without a common letter differ, $P < 0.05$.

Fig. 7. Concurrent mTOR pathway activation and VEGF production in ACC. **A**, immunohistochemical staining of p-TSC2, p-mTOR, p-S6 as well as VEGF in both NSG and ACC tissues. **B**, double-labeling immunofluorescence histochemistry of p-S6 and VEGF in both NSG and ACC tissues.

JPET Fast Forward. Published on May 18, 2010 as DOI: 10.1124/jpet.110.167692
This article has not been copyedited and formatted. The final version may differ from this version.

TABLE 1

Spearman rank test analyses of immunostainings

Marker	p-mTOR	p-S6	VEGF	MVD
p-TSC2	n=56 ($P < 0.005$)	n=56 ($P < 0.005$)	n=56 ($P < 0.05$)	n=56 ($P < 0.05$)
p-mTOR		n=56 ($P < 0.001$)	n=56 ($P < 0.005$)	n=56 ($P < 0.01$)
p-S6			n=56 ($P < 0.001$)	n=56 ($P < 0.01$)
VEGF				n=56 ($P < 0.001$)

The values represent number of cases analyzed (n) and *P* values.

Figure 1

JPET Fast Forward. Published on May 18, 2010 as DOI: 10.1124/jpet.110.167692
This article has not been copyedited and formatted. The final version may differ from this version.

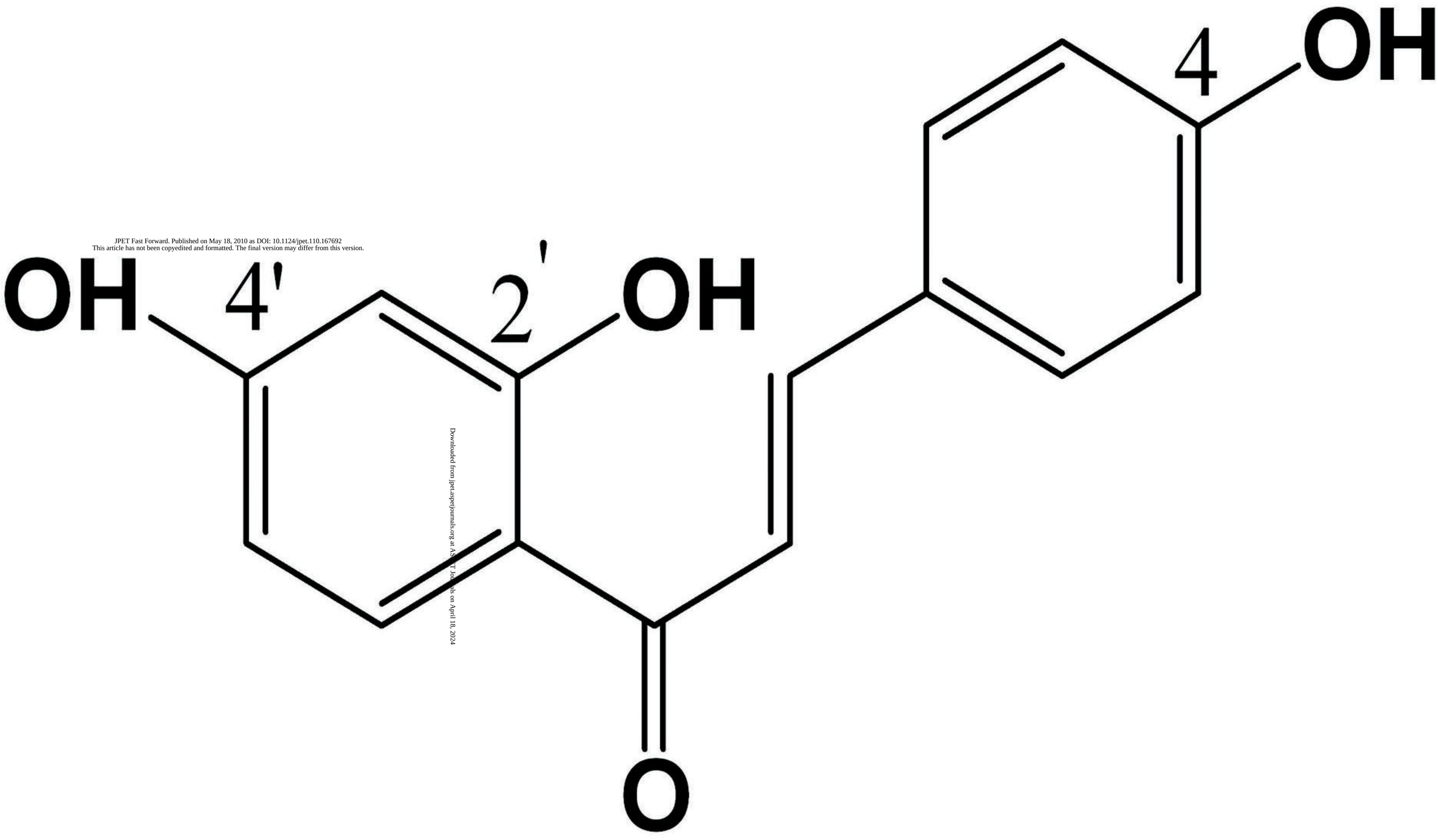

Figure 2

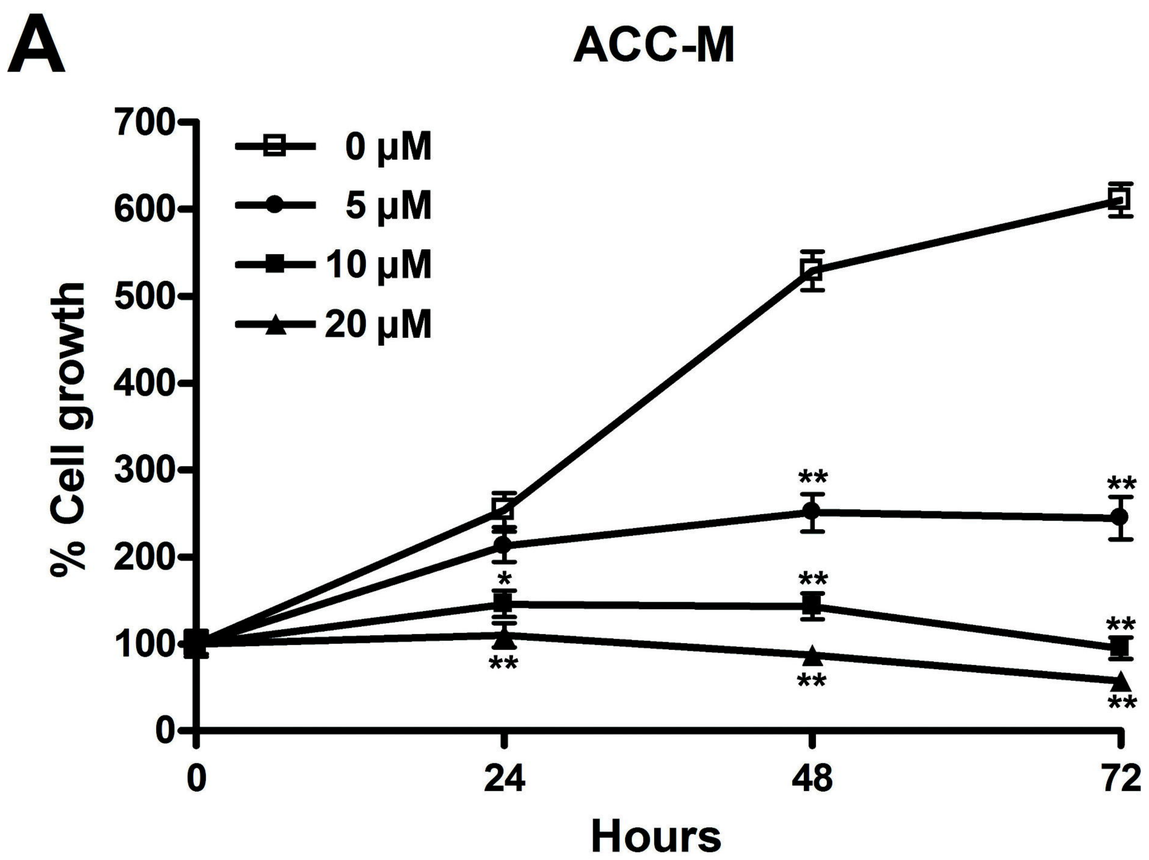
A
ACC-M
0 μM
5 μM
10 μM
20 μM
% Cell growth
Hours
0
24
48
72
100
200
300
400
500
600
700
*
**

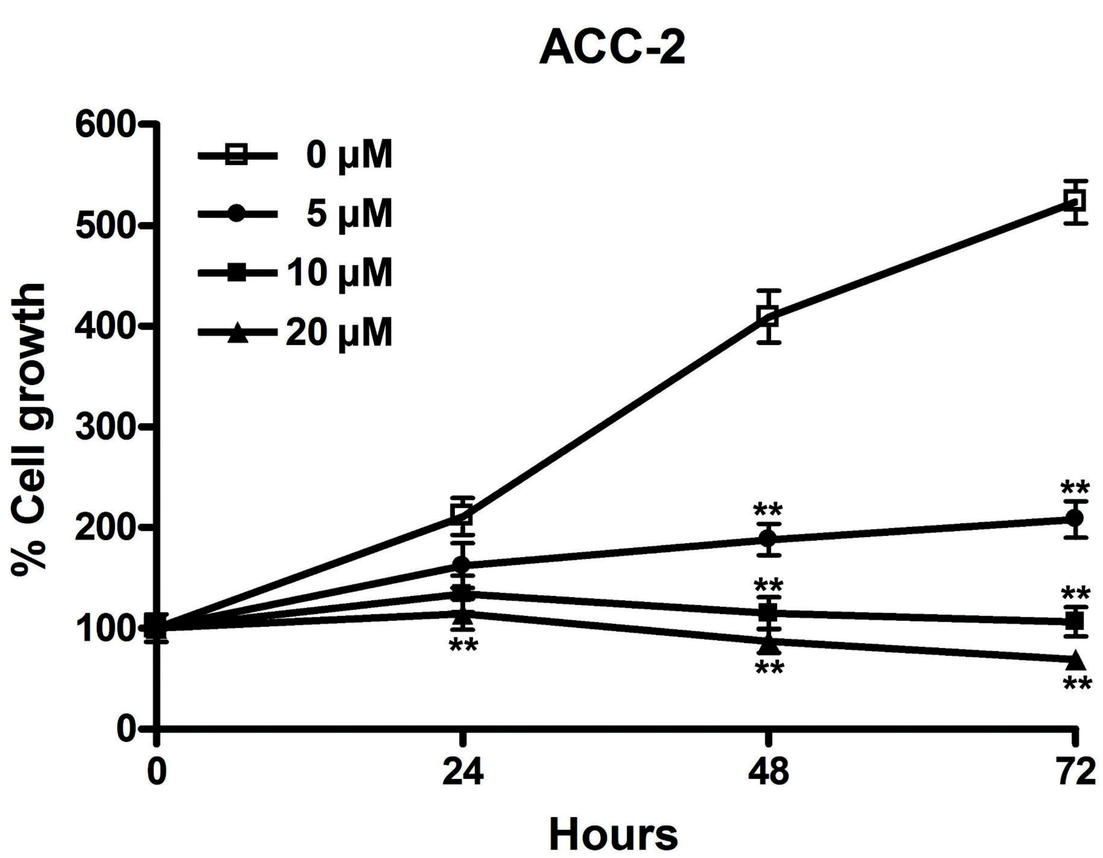
B
ACC-2
0 μM
5 μM
10 μM
20 μM
% Cell growth
Hours
0
24
48
72
100
200
300
400
500
600
**

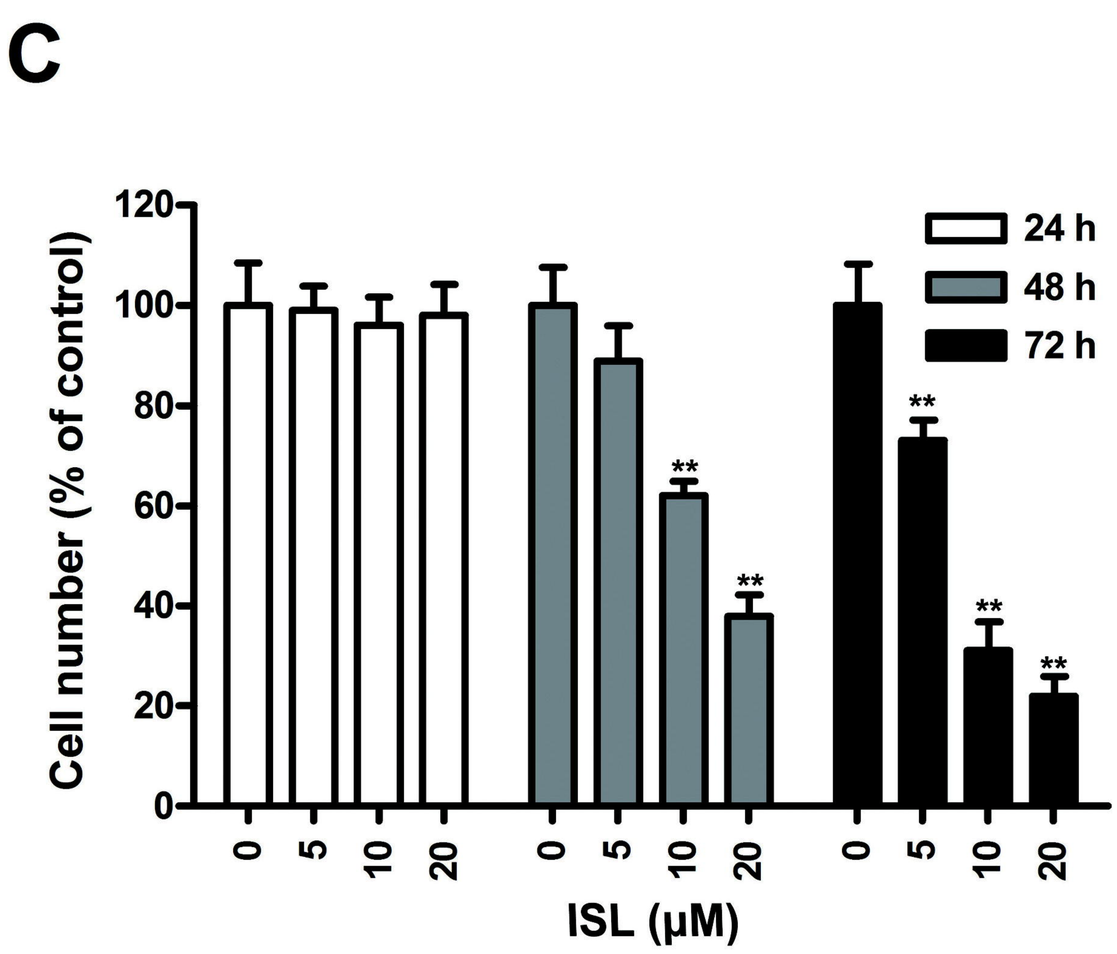
C
24 h
48 h
72 h
Cell number (% of control)
ISL (μM)
0
5
10
20
40
60
80
100
120
*
**

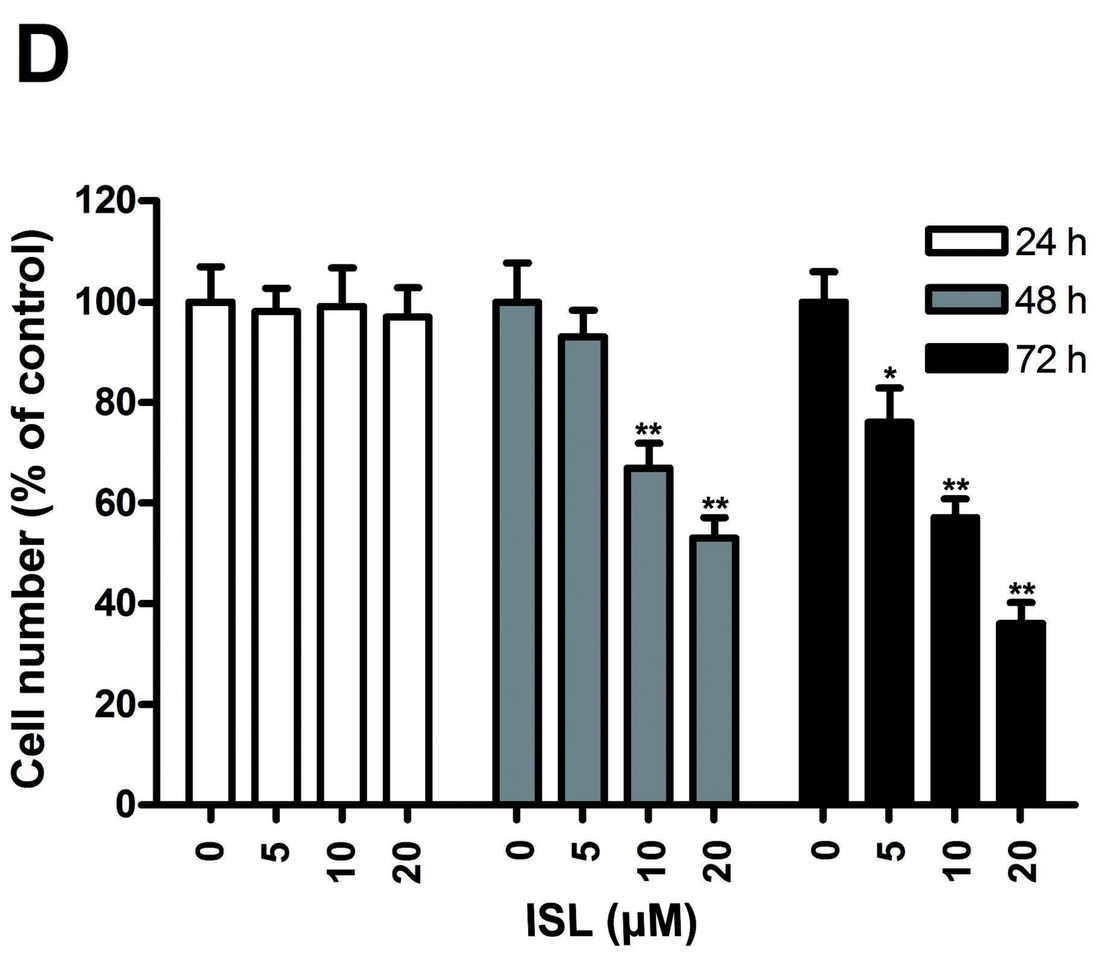
D
24 h
48 h
72 h
Cell number (% of control)
ISL (μM)
0
5
10
20
40
60
80
100
120
*
**

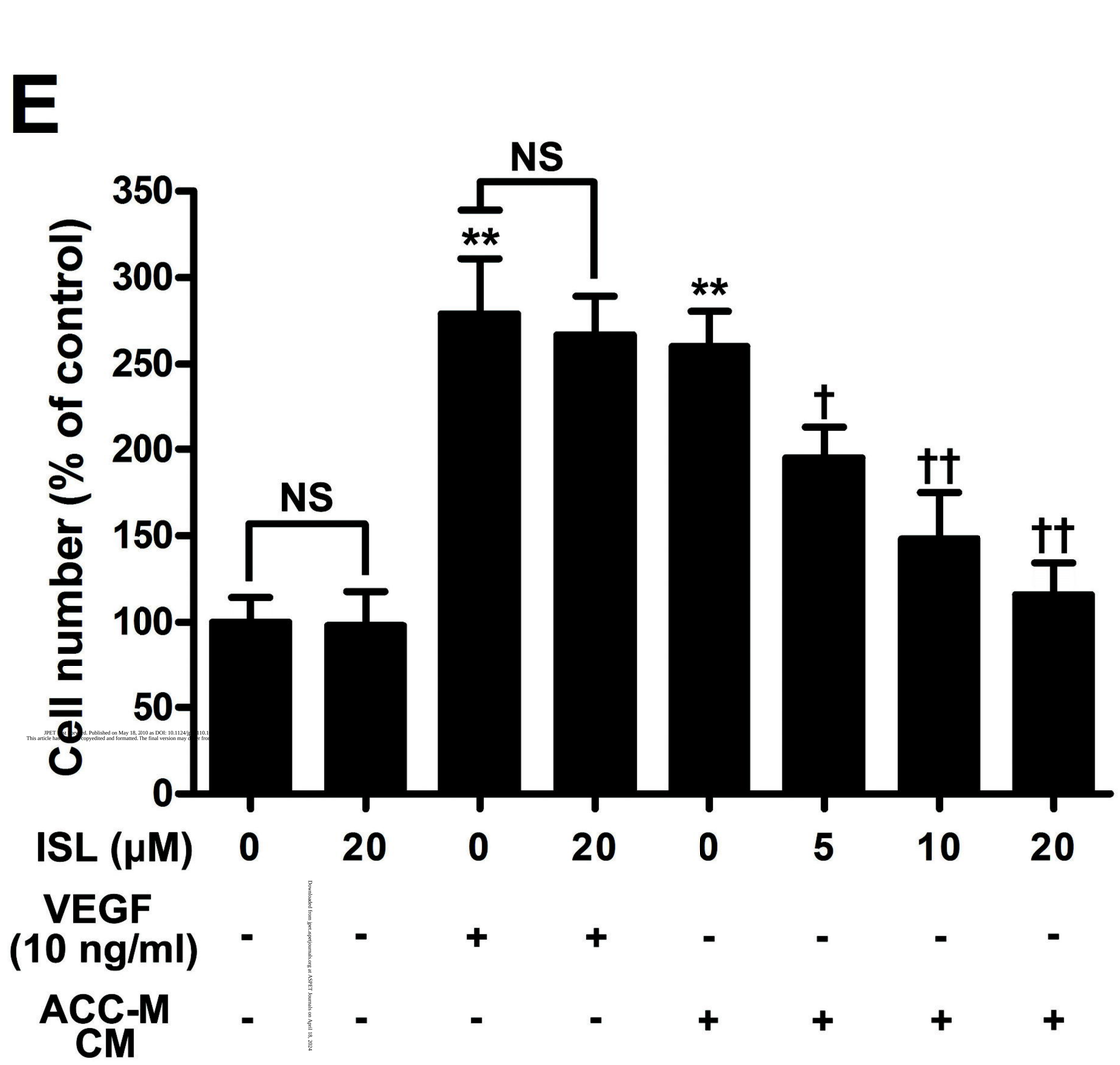
E
Cell number (% of control)
NS
**
†
††
ISL (μM)
0
20
5
10
VEGF (10 ng/ml)
ACC-M CM
-
+

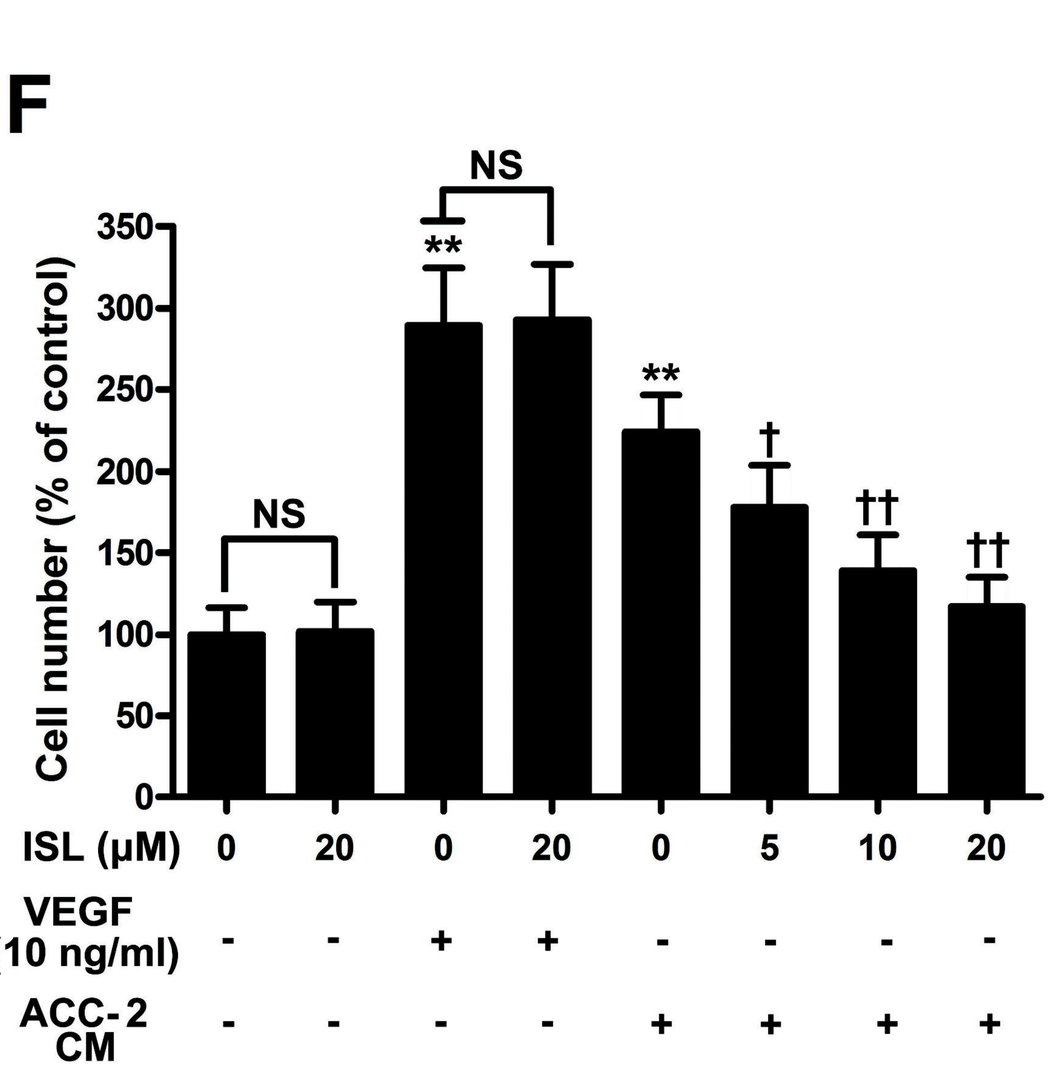
F
Cell number (% of control)
NS
**
†
††
ISL (μM)
0
20
5
10
VEGF (10 ng/ml)
ACC-2 CM
-
+

Figure 3

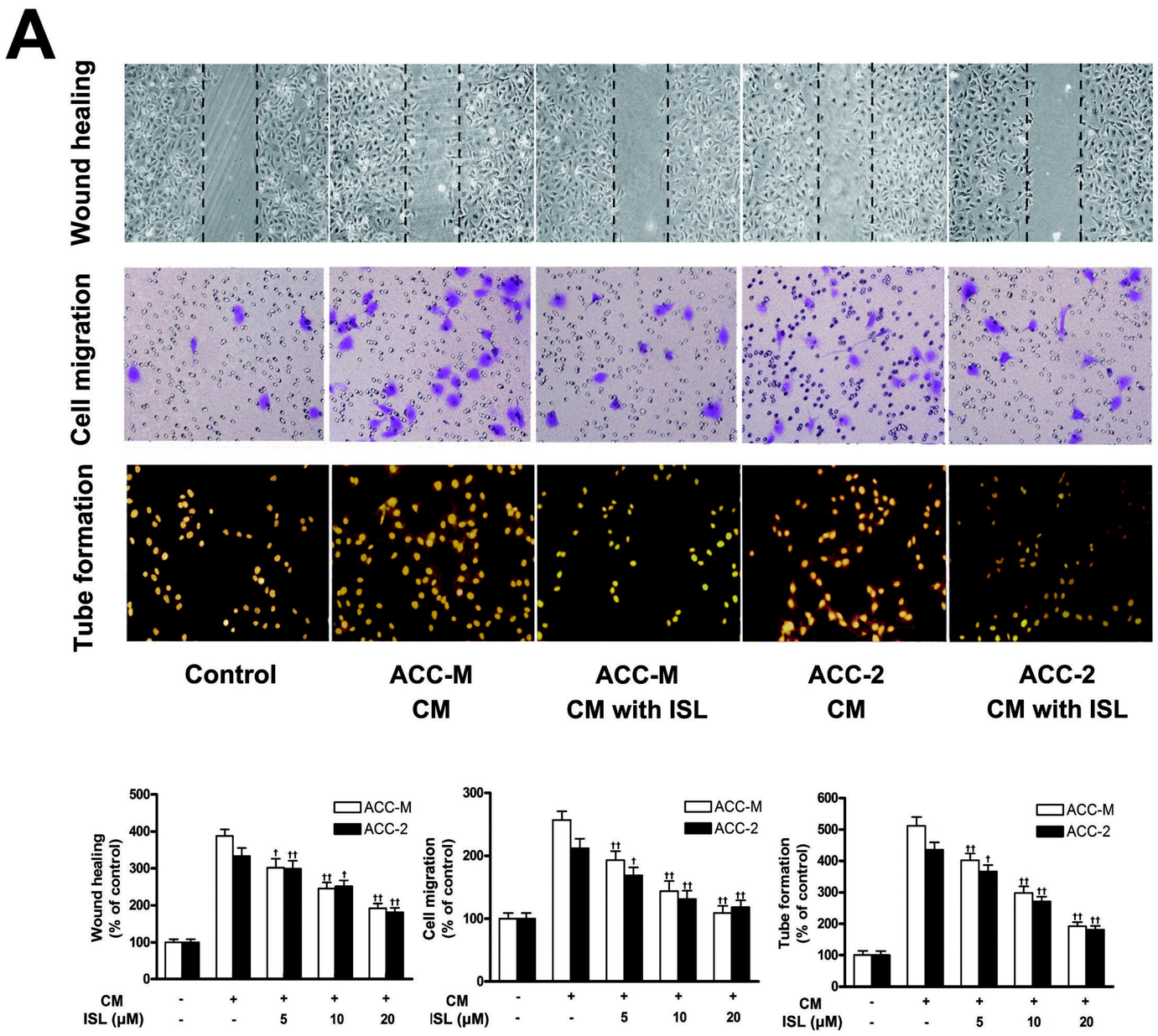
A
Wound healing
Cell migration
Tube formation
Control
ACC-M
CM
ACC-M
CM with ISL
ACC-2
CM
ACC-2
CM with ISL
Wound healing (% of control)
Cell migration (% of control)
Tube formation (% of control)
ACC-M
ACC-2
CM
ISL (μM)
B
Wound healing
Cell migration
Tube formation
Control
ISL (20μM)
VEGF (10 ng/ml)
Wound healing
Cell migration
Tube formation
% of control
NS
Control
ISL
VEGF
VEGF+ISL

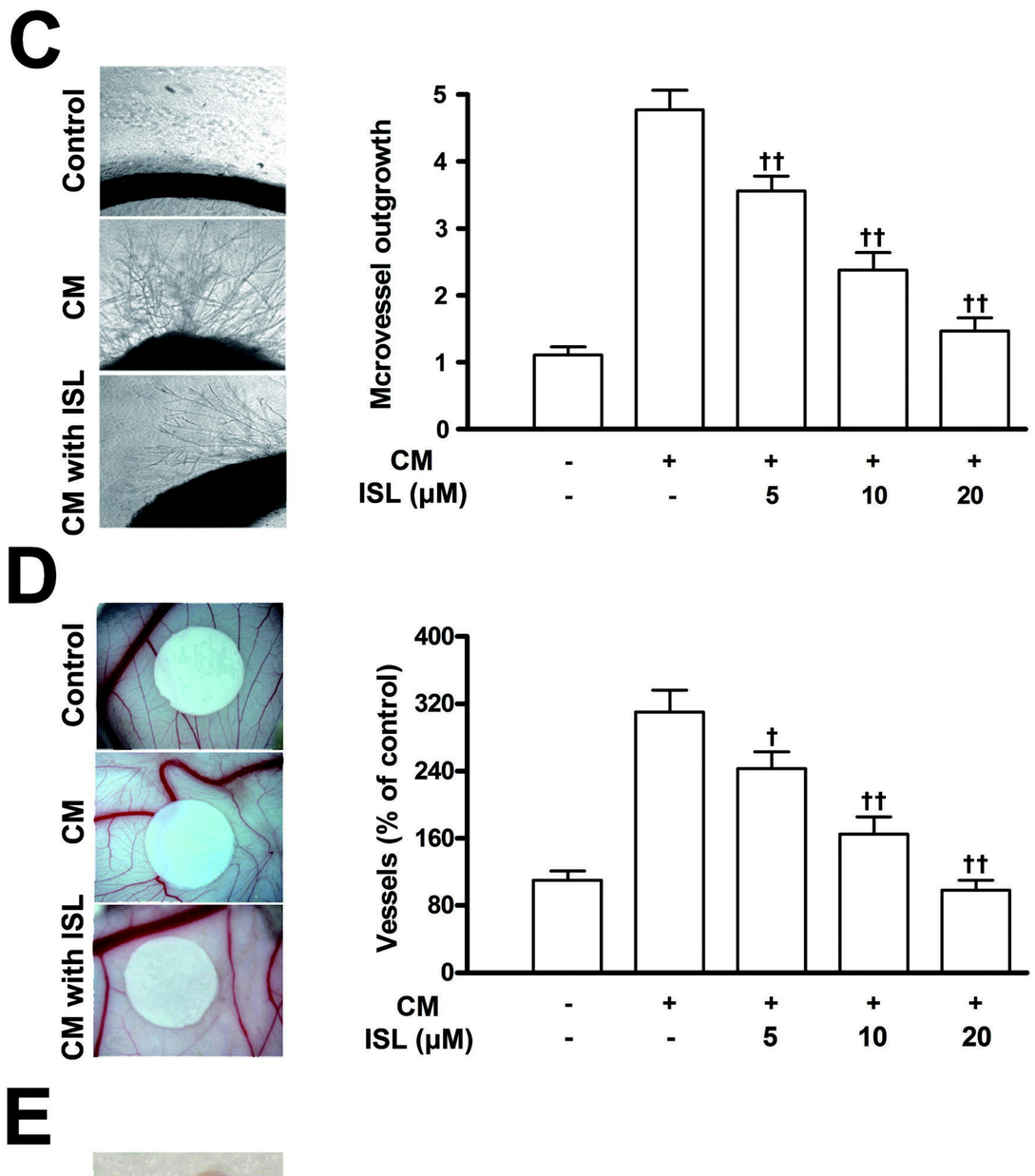
C
Control
CM
CM with ISL
Mcrovessel outgrowth
CM
ISL (μM)
D
Control
CM
CM with ISL
Vessels (% of control)
CM
ISL (μM)
E
Control
CM
CM with ISL
Hemoglobin contents (g/dL)
CM
ISL (μM)

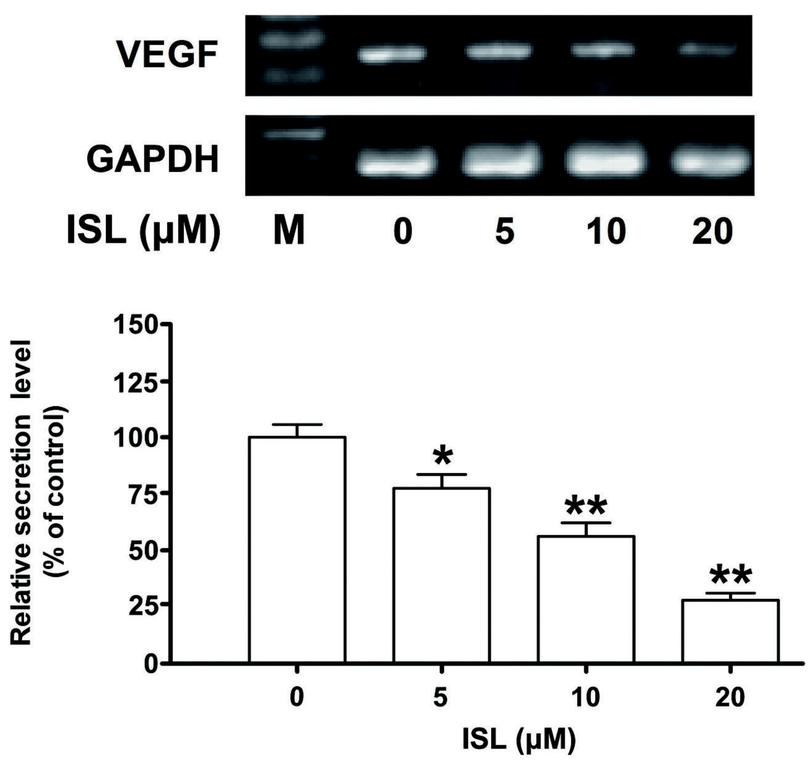
F
VEGF
GAPDH
ISL (μM)
M
0
5
10
20
G
Relative secretion level (% of control)
ISL (μM)

Figure 4

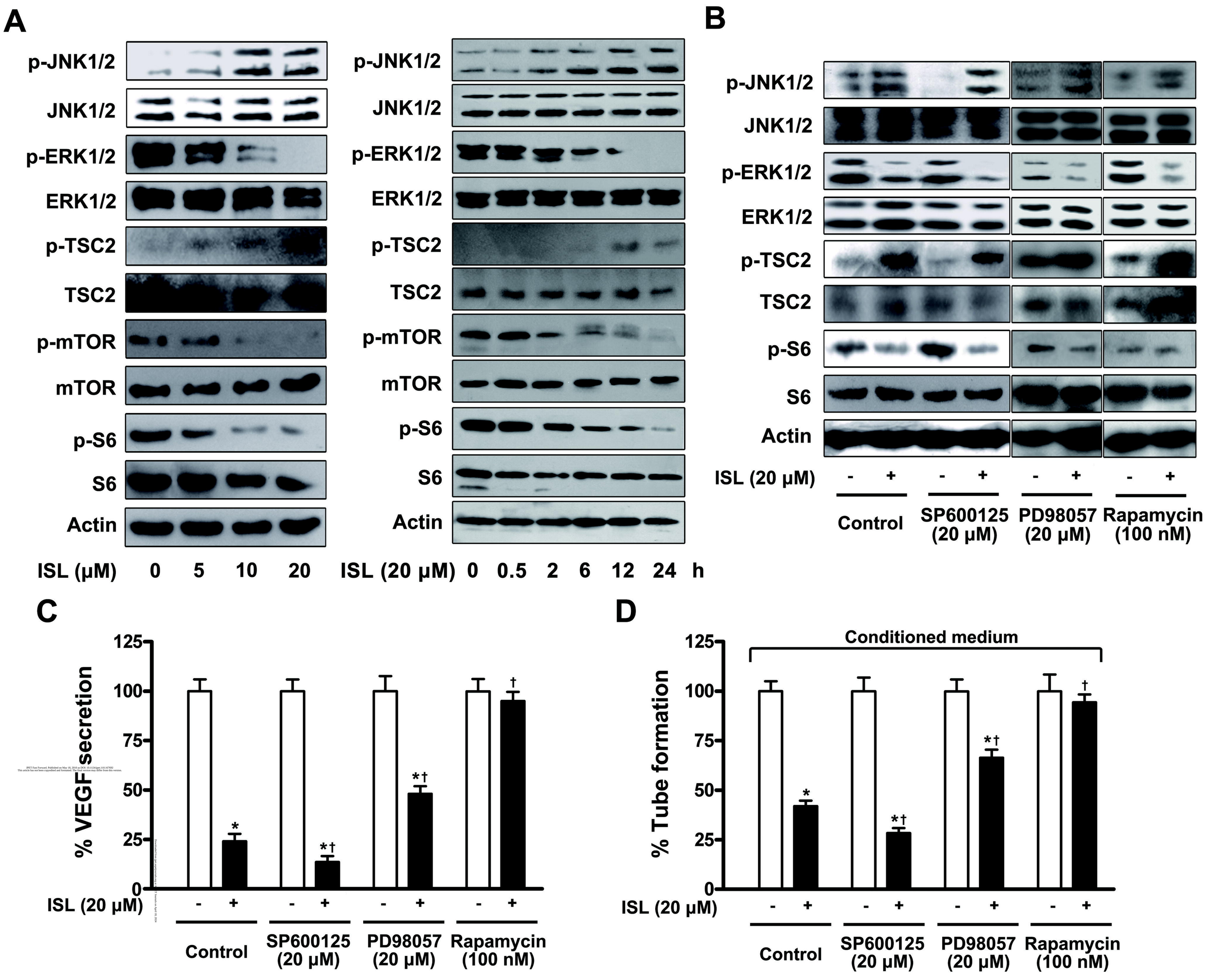

Figure 5

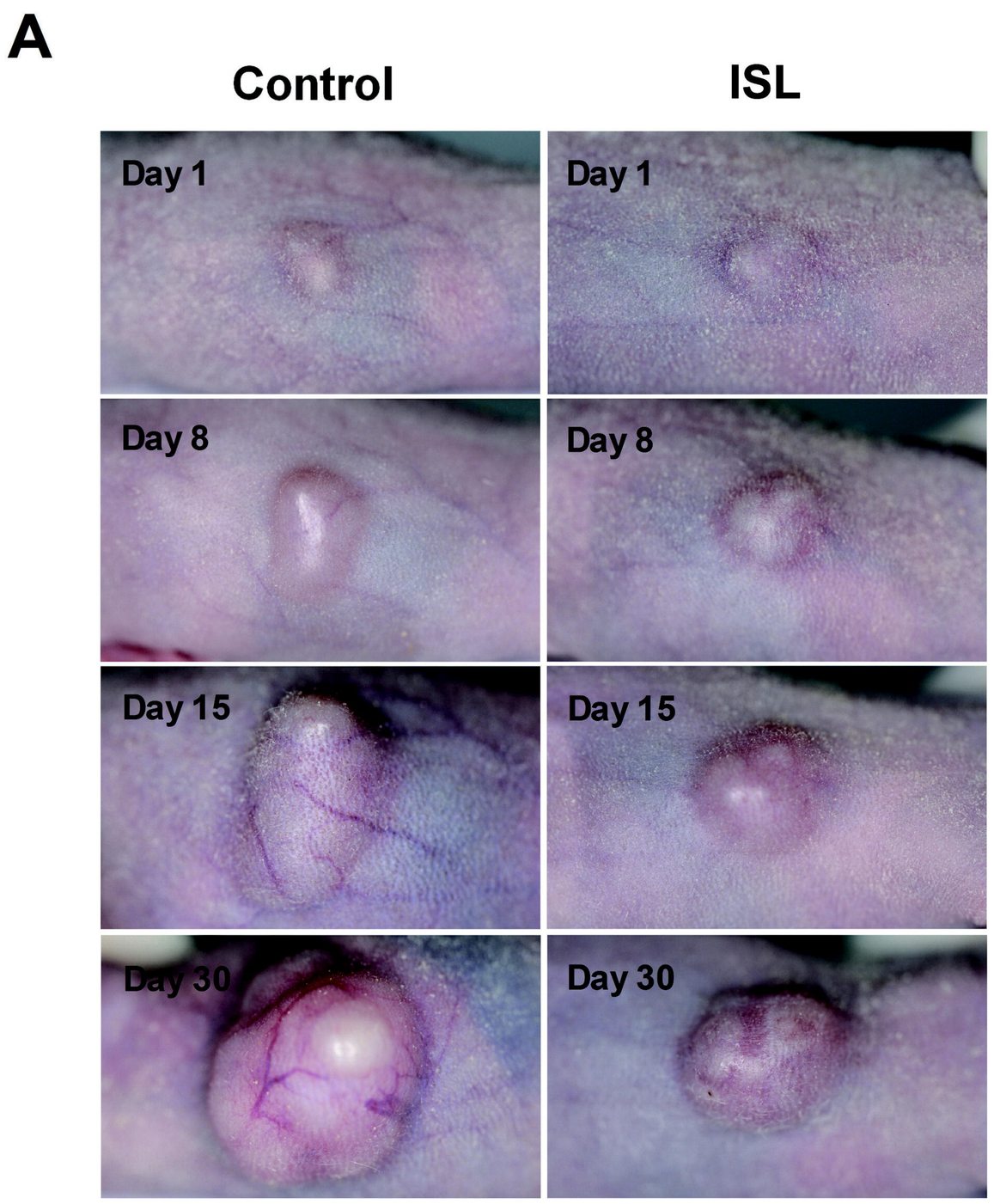
A
Control
ISL
Day 1
Day 1
Day 8
Day 8
Day 15
Day 15
Day 30
Day 30

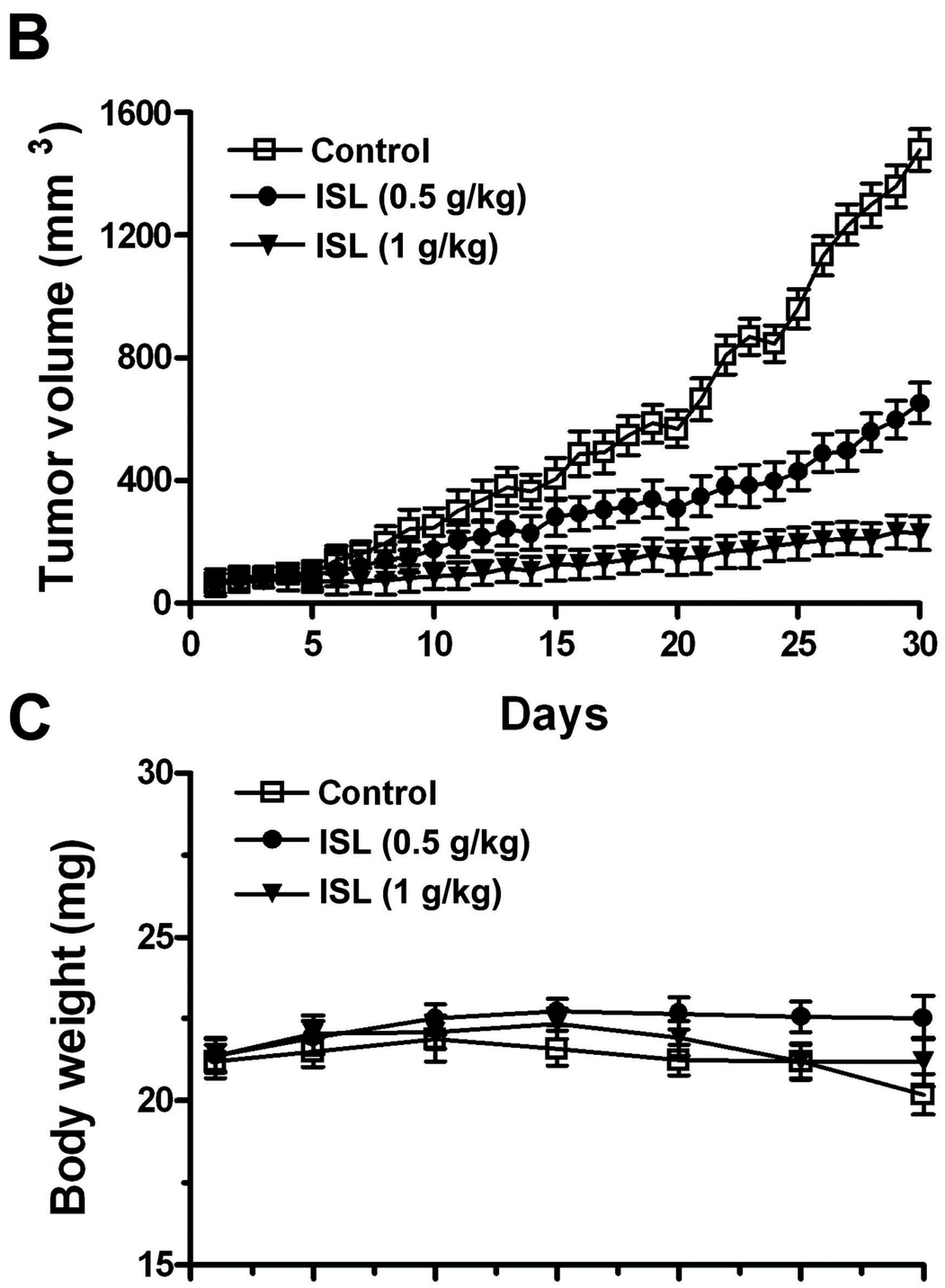
B
Tumor volume (mm 3)
1600
1200
800
400
0
Control
ISL (0.5 g/kg)
ISL (1 g/kg)
0
5
10
15
20
25
30
Days
C
Days
Body weight (mg)
30
25
20
15
Control
ISL (0.5 g/kg)
ISL (1 g/kg)
0
5
10
15
20
25
30
Days

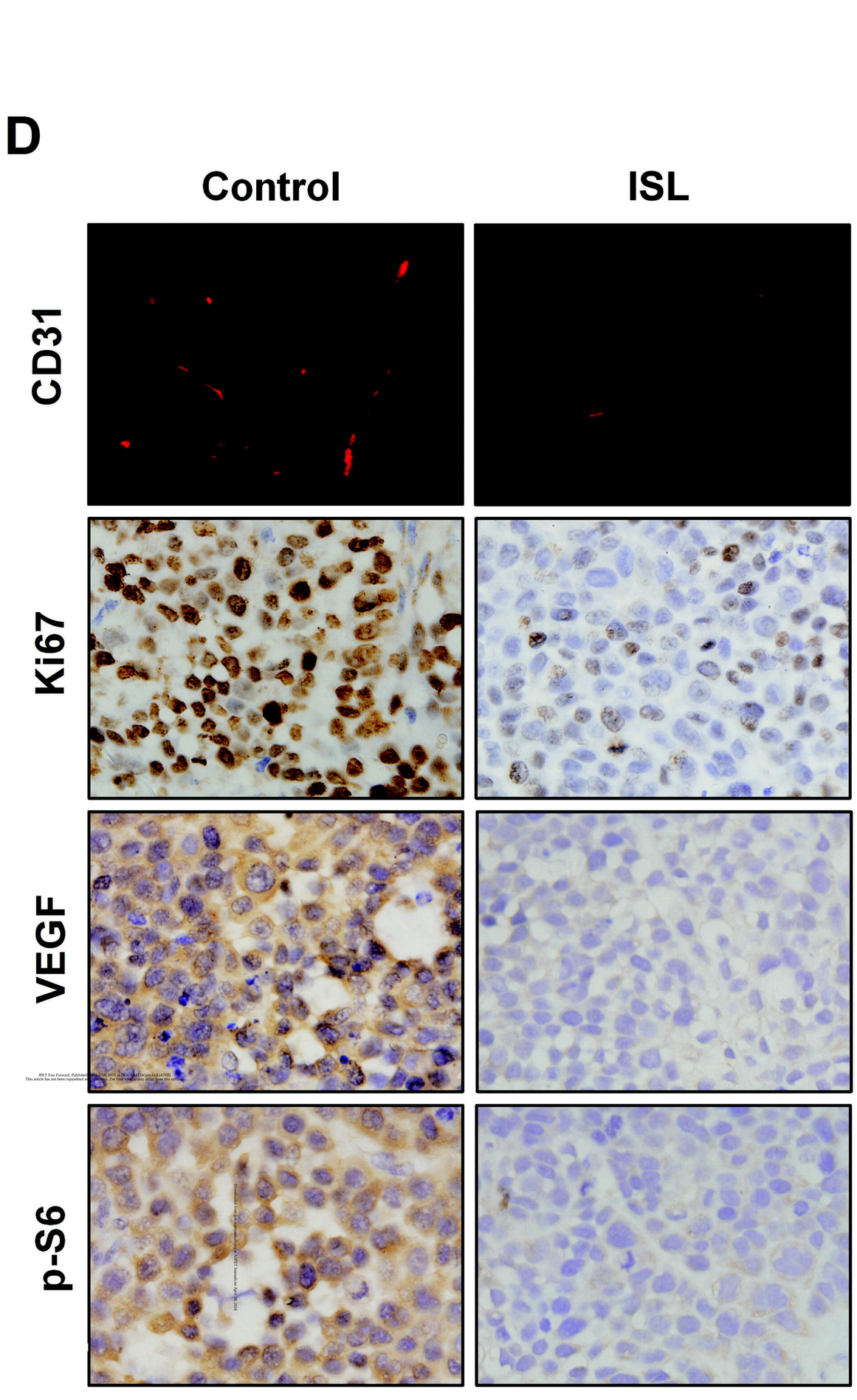
D
Control
ISL
CD31
Ki67
VEGF
p-S6

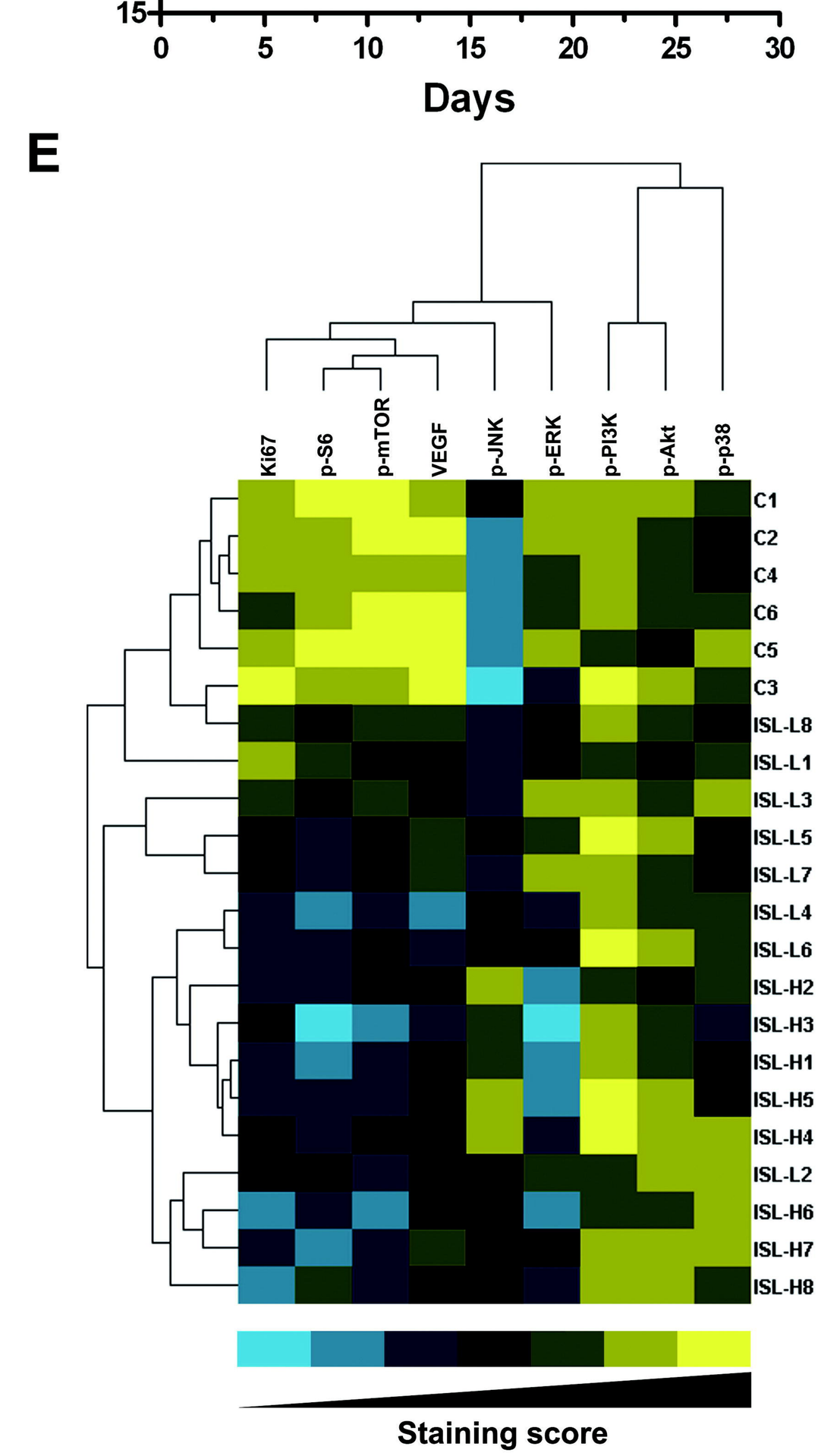
E
Ki67
p-S6
p-mTOR
VEGF
p-JNK
p-ERK
p-PI3K
p-Akt
p-p38
C1
C2
C4
C6
C5
C3
ISL-L8
ISL-L1
ISL-L3
ISL-L5
ISL-L7
ISL-L4
ISL-L6
ISL-H2
ISL-H3
ISL-H1
ISL-H5
ISL-H4
ISL-L2
ISL-H6
ISL-H7
ISL-H8
Staining score

Figure 6

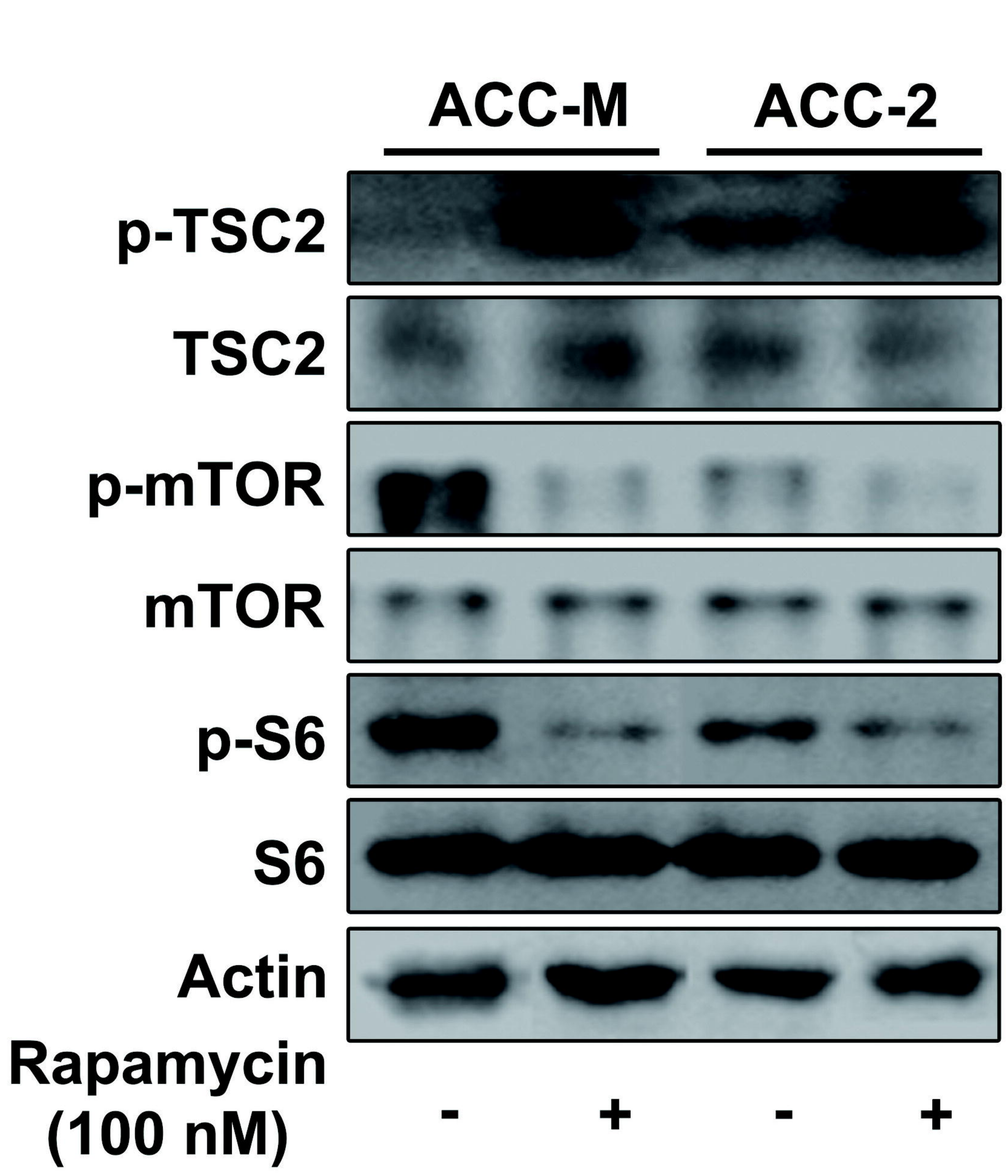

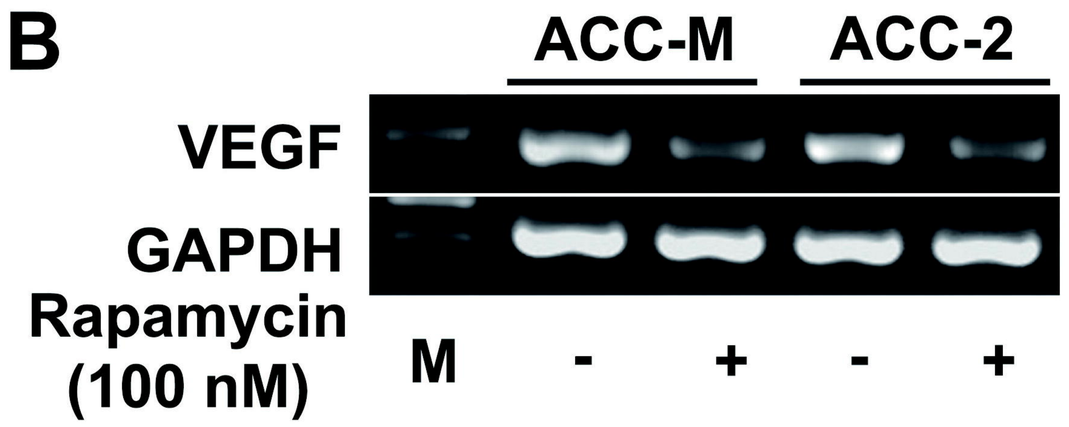

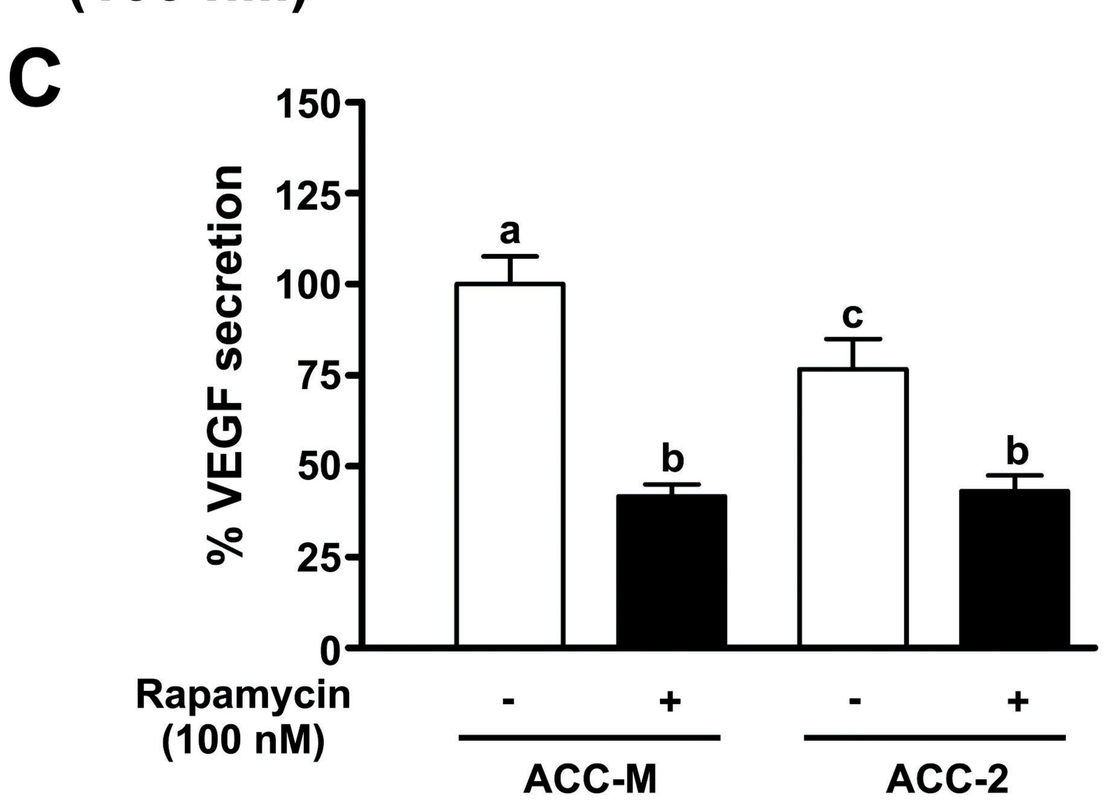

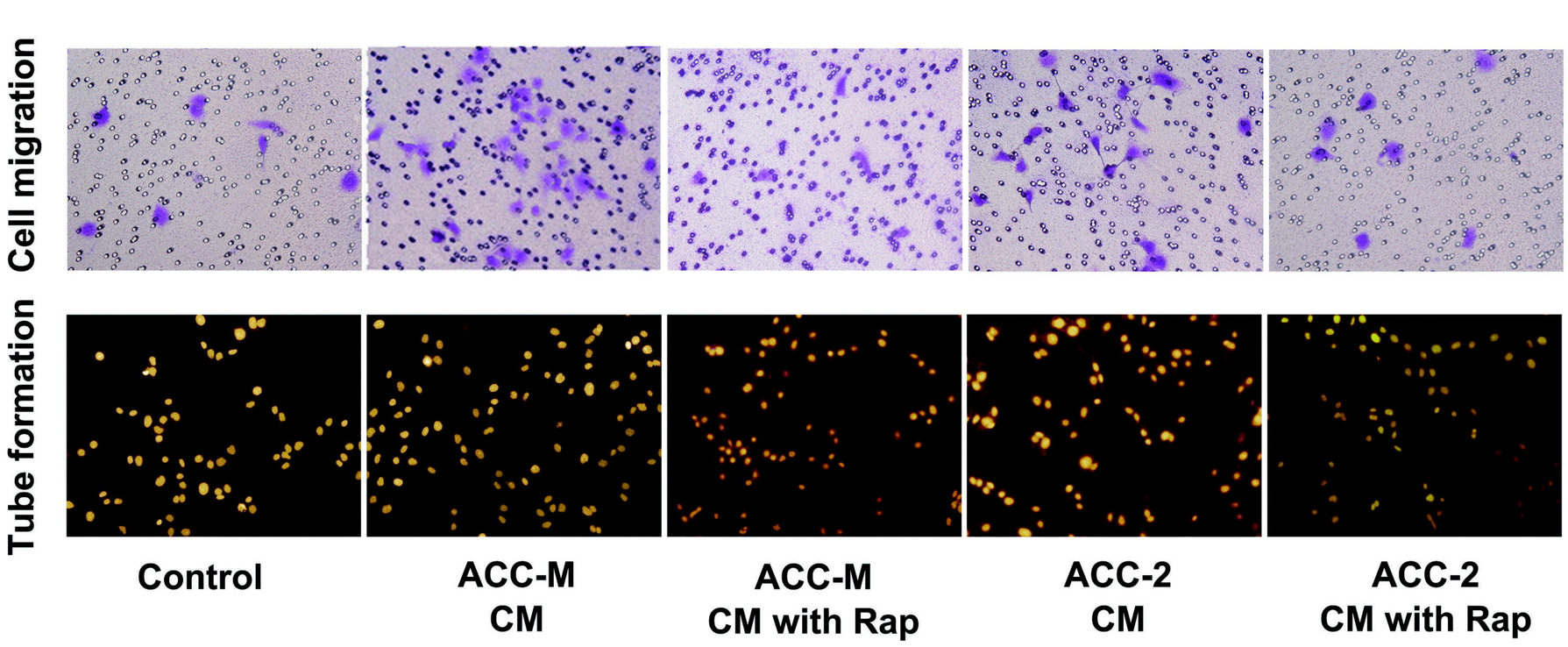

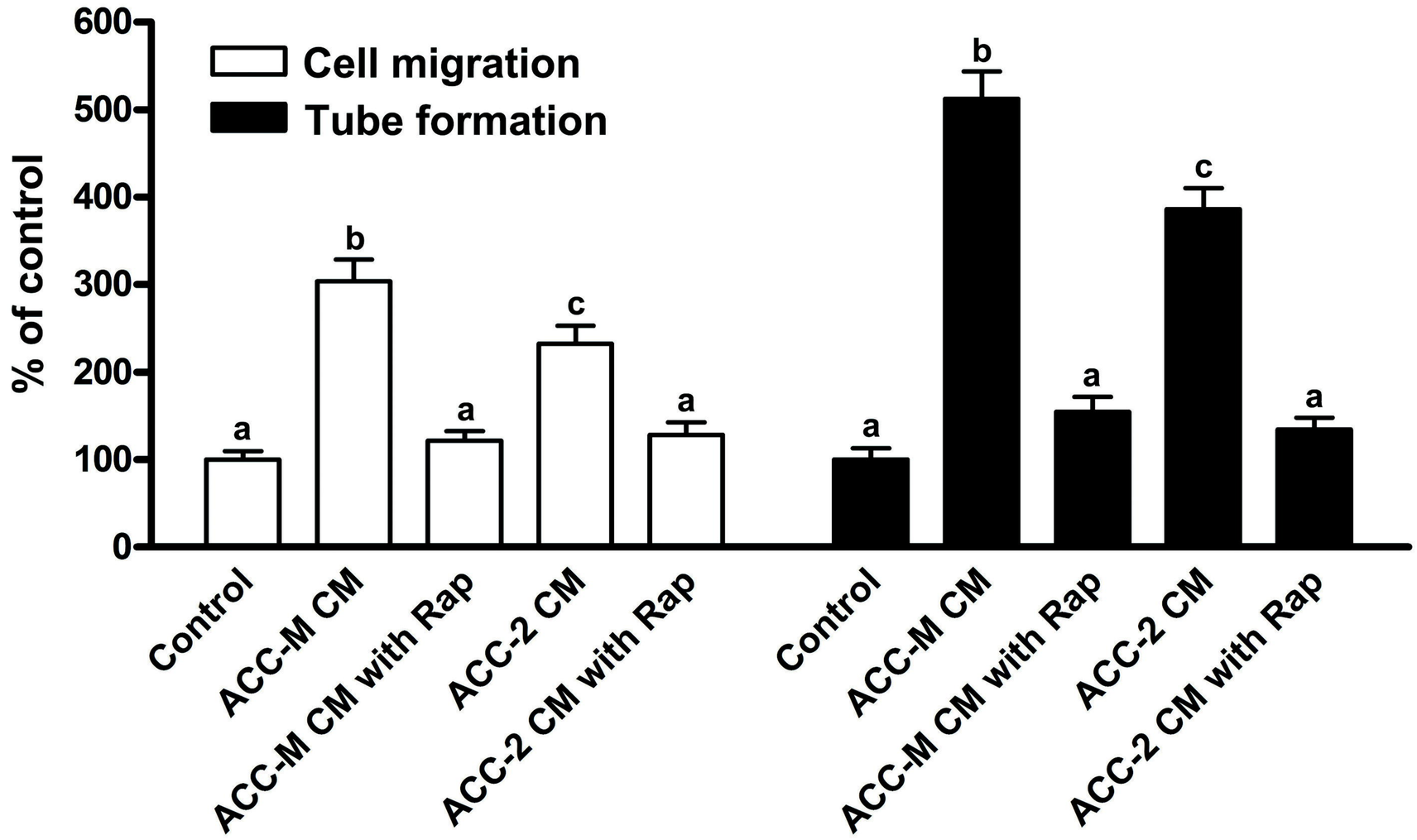

JPET Fast Forward. Published on May 18, 2010 as DOI: 10.1124/jpet.110.167692
This article has not been copyedited and formatted. The final version may differ from this version.

Figure 7